The Meteoritical Society

Meteoritics & Planetary Science 55, Nr 4, 936–961 (2020)
doi: 10.1111/maps.13454

Ramgarh, Rajasthan, India: A 10 km diameter complex impact structure

Thomas KENKMANN[1,*], Gerwin WULF[1], and Amar AGARWAL[1,2]

[1]Institute of Earth and Environmental Sciences—Geology, Albert-Ludwigs-Universität Freiburg, Albertstrasse 23-B, 79104 Freiburg im Breisgau, Germany
[2]Department of Earth Sciences, Indian Institute of Technology-Kanpur, Kanpur-208016, India
Corresponding author: E-mail: Thomas.kenkmann@geologie.uni-freiburg.de

(Received 14 June 2019; revision accepted 26 January 2020)

Abstract–The Ramgarh structure is a morphological landmark in southeastern Rajasthan, India. Its 200 m high and 3.5–4 km wide annular collar has provoked many hypotheses regarding its origin, including impact. Here, we document planar deformation features, planar fractures, and feather features in quartz grains of the central part of the Ramgarh structure, which confirm its impact origin. The annular collar does not mark the crater rim but represents the outer part of a central uplift of an approximately 10 km diameter complex impact structure. The apparent crater rim is exposed as a low-angle normal fault and can be traced as lineaments in remote sensing imagery. The central uplift shows a stratigraphic uplift of ~1000 m and is rectangular in shape. It is dissected by numerous faults that are co-genetic with the formation of the central uplift. The central uplift has a bilateral symmetry along an SW-NE axis, where a large strike-slip fault documents a strong horizontal shear component. This direction corresponds to the assumed impact trajectory from the SW toward the NE. The uprange sector is characterized by concentric reverse faults, whereas radial faults dominate downrange. Sandstones of the central uplift are infiltrated by Fe-oxides and suggest an impact-induced hydrothermal mineralization overprint. The impact may have occurred into a shallow water environment as indicated by soft-sediment deformation features, observed near the apparent crater rim, and the deposition of a diamictite layer above them. Gastropods embedded in the diamictite have Middle Jurassic age and may indicate the time of the impact.

INTRODUCTION

The number of impact craters on a planetary surface depends on the rate of impact crater production and the rate of resurfacing. The Earth is characterized by a high resurfacing rate and consequently has a relatively low number of well-preserved impact craters. Terrestrial craters are affected by erosion, tectonics, sedimentation, and burial. Such processes not only reduce their total number but also affect their morphological appearance. Whereas only a few of the younger impact craters are relatively well preserved and only slightly degraded, older crater structures commonly have subdued morphologies or cannot be recognized anymore.

As the morphological appearance is commonly transient, the discovery and confirmation of terrestrial impact structures rely on the recognition and the proper documentation of shock indicators (French 1998; French and Koeberl 2010). Currently, 204 craters will be listed in the Atlas of Terrestrial Impact Structures (Gottwald, personal communication). Taking the mean erosion rate for the Earth and the crater production function of the Moon adopted for the Earth, some additional 200 impact structures still await discovery (Hergarten and Kenkmann 2015). Here, we report on the Ramgarh structure in Rajasthan, India. Its impact origin, which has long been controversial, could be confirmed by shock effects, and consequently, the structure should be regarded as the third impact crater recognized on the Indian subcontinent.

Ramgarh is a well-known morphological landmark (Fig. 1) in a flat sedimentary terrain of southeastern Rajasthan, India. This structure has been a focus of scientific investigation and controversial debate among

Indian geologists since the nineteenth century. The 3.5–4 km diameter annular feature rises some 200 m above the surrounding flat plain. Geological interpretations of the structure included scenarios of a dome-like uplift induced by a combination of a magmatic intrusion and tectonic forcing (Sharma 1973), an origin by a volcanic explosion or as a kimberlite pipe (Balasundaram and Dube 1973), diapirism (Crawford 1972), or an origin by an impact event (e.g., Crawford 1972; Rakshit 1973; Ahmed et al. 1974; Sisodia et al. 2006; Rana and Agarwal 2016; Kenkmann et al. 2019; Misra et al. 2019). A more exotic explanation is the subterranean centripetal flow of shales proposed by Ramasamy (1987, 1988). The impact scenario is the one favored nowadays by most researchers. Several attempts have been carried out in the past decades to prove the impact hypotheses. The finding of shock features including planar deformation features (PDFs) and planar fractures (PFs) in quartz grains has repeatedly been claimed (Master and Pandit 1999; Sisodia et al. 2006; Das et al. 2011; Purohit and Sisodia 2013; Rana and Agarwal 2016; Dutta et al. 2018) but remained debated (Reimold et al. 2006). The most convincing shock features presented so far have been those from Rana and Agarwal (2016; figs. 2A and 2D) and Kenkmann et al. (2019).

With the exception of Rakshit (1973) and Dietz and McHone (1974), all previous studies that suggested an impact origin for Ramgarh interpreted the 3.5–4 km wide morphological ring as the rim of the crater (e.g., Sisodia et al. 2006; Misra et al. 2008; Rana and Agarwal 2016; Dutta et al. 2018). A tiny hill in the center of the depression with a height of ~6 m and a base width of ~20 m was considered by some of the authors as a central peak. Here, we show that the remarkable morphological annular collar of Ramgarh is not the rim of an impact crater but represents the outer part of a central uplift of a considerably larger impact structure, as originally suggested by Rakshit (1973) and Dietz and McHone (1974). We demonstrate that the impact structure has an apparent diameter of approximately 10 km (Fig. 1). The crater rim of Ramgarh is morphologically hardly recognizable, but it is defined by shallowly inward dipping normal faults that strike concentrically with respect to the center of the annular feature, and concentric lineaments traceable through the Quaternary cover. We discuss that the Ramgarh impact structure may have formed in shallow water during the Middle Jurassic.

HISTORY OF INVESTIGATION OF THE RAMGARH STRUCTURE

The area around Ramgarh was first mapped in 1869 (Mallet 1869); however, the structure was overlooked at that time. Based on an unpublished map by Kishen Singh that is dated to 1881–1882 (Rakshit 1973), the Geological Survey of India favored a dome structure induced by an intrusion as the most likely explanation for the structure. Later, the structure was compared with a kimberlite pipe east of Allahabad, India (Ramasamy 1987). In 1969–1970, Sharma and Singh (1970) conducted two magnetic and two refraction seismic traverses in the central crater depression. Their results and the inferred magnetic anomalies did not yield any indication of an intrusive body underneath. Likewise, the regional aeromagnetic anomaly map does not show any magnetic high below the structure, which may have indicated an intrusion (Kumar et al. 2011). The absence of volcanic or intrusive rocks at the Ramgarh structure was further confirmed by a 452 m deep borehole drilled in 1981–1982 into the center of the structure (Ramasamy 1988).

Based on remote sensing imagery, Crawford (1972) speculated about an anomalous tectonic origin, possibly caused by diapirism. Evidently, he was the first to favor an impact scenario and reported a possible shatter cone in colluvium of the central depression. However, this finding could not be substantiated by subsequent investigations. Crawford (1972) was unaware of the geological mapping of the site by the Geological Survey of India in 1971–1972 (Rakshit 1973). In this report, several possible hypotheses for the origin of Ramgarh were discussed including the presence of intrusive rock at depth, a volcanic crater scenario, tectonic forcing, diapirism, and an impact origin. Sharma (1973), who documented the domal structure with quaquaversal dips, preferred a combination of volcanic and tectonic processes responsible for the observed structural uplift. Balasundaram and Dube (1973) found numerous and closely spaced fractures in quartz grains of the Lower Bhander Sandstone and supported the impact hypothesis, although the microstructural findings were inconclusive. The same postulations were published by Ahmed et al. (1974) and later by Khan (1980), though none of them could prove the impact hypothesis. Ramasamy (1987) suggested that the dome structure was formed by some sort of subsurface flow of shales caused by lateral compression.

Using early satellite imagery of the Earth Resources Technology satellite (ERTS-1), Dietz and McHone (1974) listed Ramgarh as a possible impact structure and suggested that the structure probably represents a central uplift of a much larger crater. Further remote sensing studies were carried out by Murali and Williams (1990) and Murali and Lulla (1992) based on multispectral data of the Indian Remote Sensing satellite (IRS-1A). They identified faults crossing the annular ring of Ramgarh and interpreted them as

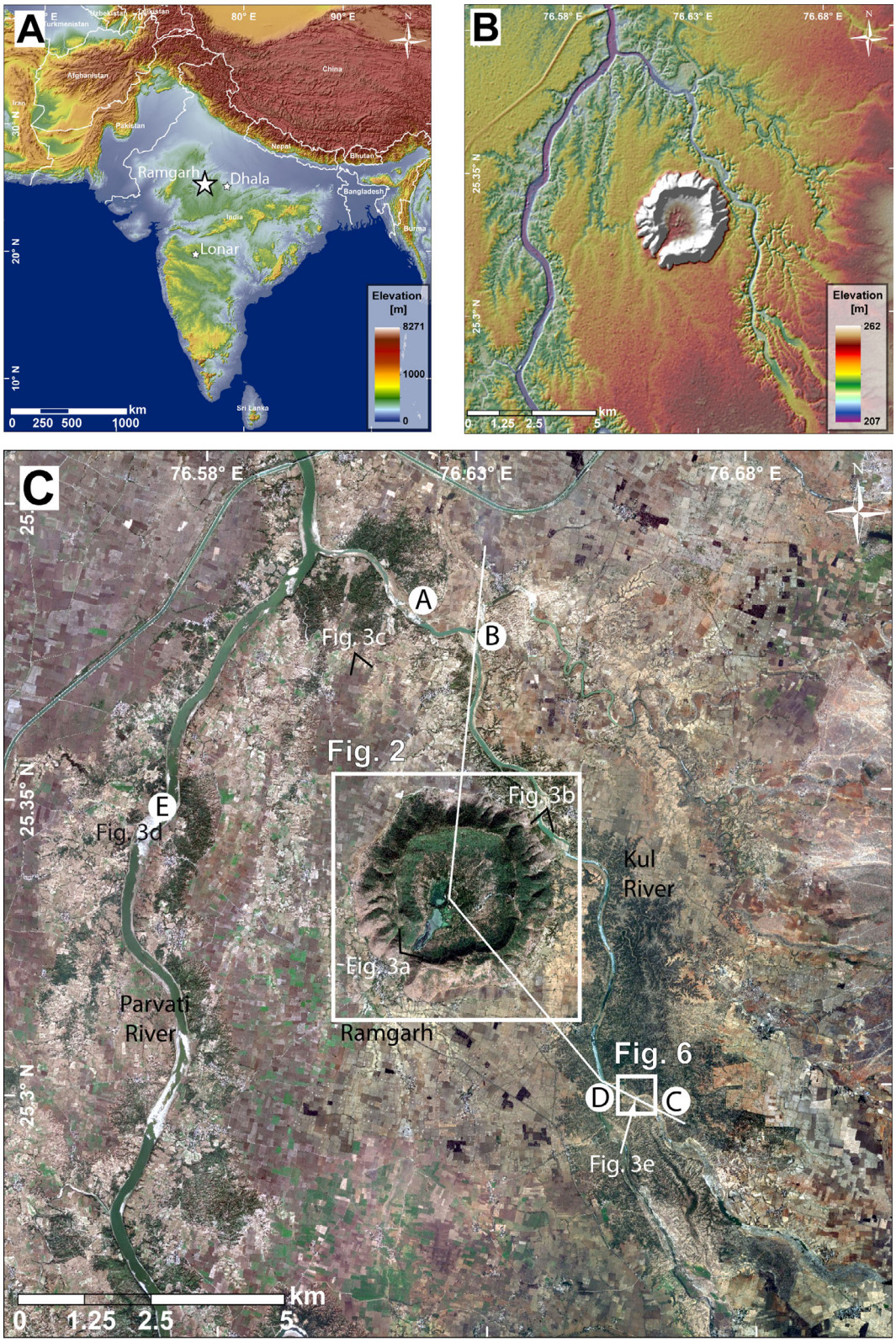

Fig. 1. A) Map showing the location of the Ramgarh structure in India (ETOPO1 DEM superposed on 15x vertically exaggerated ETOPO1 shaded relief). B) Elevation map of the Ramgarh structure (76.624°E, 25.332°N) (ALOS DEM mosaic superposed on ALOS shaded relief), and (C) satellite image of the surroundings of the Ramgarh structure showing the locations of Figs. 2, 3 and 6 and the profile line for Fig. 15 (Digital Globe imagery).

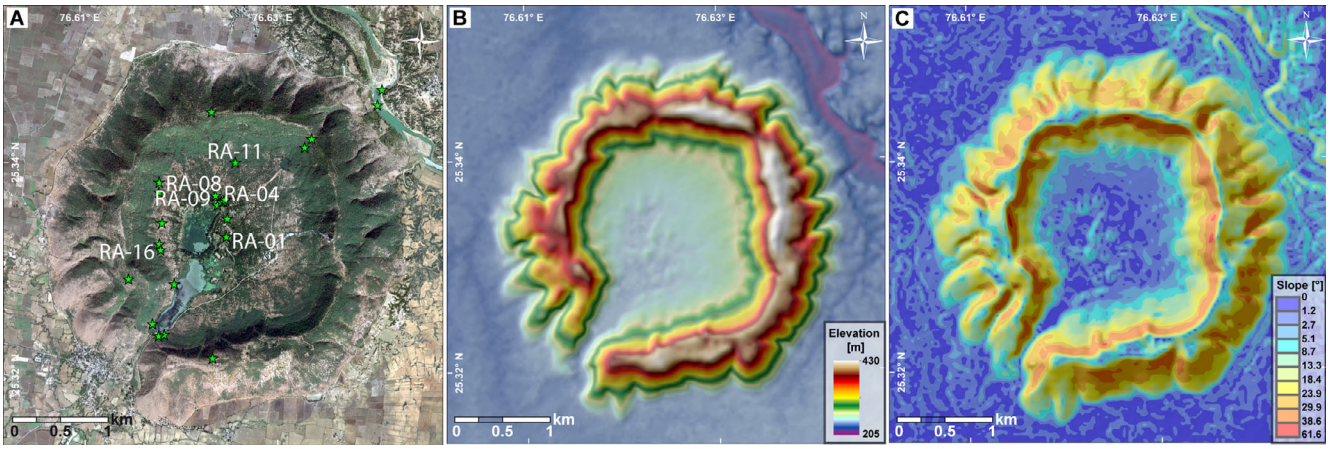

Fig. 2. Close-up view of the morphological annular collar of the Ramgarh structure showing an ~200 m high topographic landmark in otherwise flat terrain of intense agricultural use. The inner slopes of the collar are steeper than the outer flanks. A) Digital Globe imagery with locations of those sample sites that yielded shocked samples (green stars; see also Table 2). B) ALOS DEM mosaic superposed on ALOS shaded relief. C) ALOS slope map superposed on ALOS shaded relief.

young tectonic features, in accordance with Sharma (1973) and Misra et al. (2008). Recently, Pareta and Pareta (2016) and Misra et al. (2019) conducted remote sensing analyses of Ramgarh using the multispectral Advanced Space born Thermal Emission and Reflection Radiometer (ASTER), Landsat 7 and 8 imageries, and shuttle radar topographic mission (SRTM) digital elevation models to evaluate the morphology of the Ramgarh structure and its surroundings. They also concluded that the size of the potential crater coincided with the size of the morphological collar. In the surrounding of the apparent crater, they found NE-SW and NW-SE trending lineaments, which they interpreted as later tectonic strike-slip faults that crossed the collar.

At the end of the 20th century, research on Ramgarh became focused on finding the evidence for the proposed impact scenario. In a conference abstract, Master and Pandit (1999) claimed that they found one to three sets of mostly decorated PDFs in quartz grains in virtually every thin section they produced of the Lower Bhander Sandstone of the collar. These alleged findings were, however, not substantiated by photomicrographs and never published in a peer-reviewed article. Several authors claimed the finding of PFs and/or PDFs from either the Lower Bhander Sandstone or the Rewa Sandstone, among them Sisodia et al. (2006), Das et al. (2011), Purohit and Sisodia (2013), Rana and Agarwal (2016), and Dutta et al. (2018). Unfortunately, the features presented by Sisodia et al. (2006) and Purohit and Sisodia (2013) are curvilinear or show gradational transitions to the host grain typical for lattice bending and Boehm lamellae (Reimold et al. 2006). Dutta et al. (2018) showed irregularly spaced, curved, cross-cutting fracture sets and interpreted them as PFs. Das et al. (2011) showed a figure with wider spaced straight lamellae in a single quartz grain but did not index them. Rana and Agarwal (2016) showed a promising quartz grain with possible PDFs from the Rewa Sandstone in their figs. 2A and 2A, unfortunately without scale bar and crystallographic indexing. These authors also presented alleged PFs and PDFs that are twin lamellae (Rana and Agarwal 2016, fig. 2B) and deformation bands (Rana and Agarwal 2016, fig. 2C). The criteria for the proper identification, documentation, and formation of shock features have been demonstrated, for instance, in Stöffler and Langenhorst (1994); French (1998); French and Koeberl (2010); and, concerning FFs, in Poelchau and Kenkmann (2011).

Several authors also described iron-silica–rich, mm-sized magnetic spherules (Sisodia et al. 2006; Misra et al. 2008, 2013; Das et al. 2009, 2011) with very high natural remanent magnetization (NRM) of 2–19 Am^{-1} and a high Ni content of 200–4000 ppm (Misra et al. 2019) from the center of the Ramgarh structure. They interpreted them as accretionary lapilli with a component of extraterrestrial material. The high NRM was interpreted to result from shock magnetization during the impact event. Based on XRD analysis, Das et al. (2011) claimed that these accretionary lapilli contained coesite, tridymite, and cristobalite, and inferred a pressure range of > 30 GPa. Sisodia et al. (2006) and Misra et al. (2013, 2019) also observed glassy spherules with high NRM, and Dutta et al. (2018) described tear-drop–shaped melt spherules. We have to retort here that the findings of microspherules are not impact diagnostic, because similar objects can be produced by a wide range of geological and artificial

processes (French and Koeberl 2010). A large variety of glassy spherules can be produced artificially from welding spatter, coal-fired power plants, or from a variety of metallurgical and other industrial processes. Apart from this, impact spherules are commonly found in distal ejecta and are not expected to occur in the center of an eroded crater. Critique of Sisodia et al. (2006) was summarized in Reimold et al. (2006). To conclude, the research on Ramgarh has been intense, in particular in the last two decades, but the results have remained ambiguous so that the structure has not been listed as a confirmed impact crater in the Earth Impact Database (2019). The work presented here was intended to prove or disprove, beyond doubt, the impact origin of the Ramgarh structure and to contribute to the understanding of the geology of this structure.

METHODS

Our investigation is based on geological fieldwork, microscopic analysis, and remote sensing using various types of satellite imagery. Detailed fieldwork was conducted for 1 week during the dry season in December 2018. Forty-five polished thin sections of 33 rock samples were prepared and examined with a LEICA/LEITZ DMR polarizing microscope equipped with a digital camera. Shock lamellae were investigated at 500x magnification. Orientations of planar microstructures in quartz grains, including PFs, FFs, and PDFs, were measured with a LEITZ U-stage mounted onto a LEITZ polarizing microscope. Measurements were then indexed using a template for crystallographic orientations in quartz (Ferrière et al. 2009). The accuracy of U-stage measurements is estimated at ±5°. Figures were prepared with Adobe© Photoshop and Illustrator CS3. Sample locations are given in Fig. 2A.

ArcGIS 10.4 by ESRI © was used for mapping and geospatial analyses of digital elevation models (DEMs) and to analyze multispectral data. High-resolution satellite image data provided by the BaseMap function of ArcGIS 10.4 (source: Digital Globe) with a spatial resolution up to 0.3 m as well as Sentinel 2 and Landsat 5 multispectral data were used to analyze the Ramgarh structure in detail. In the process, a true color composite image of the area was generated in such a way that the Landsat 5 band ratios 5/2, 4/1, and 7/5 were assigned to the intensities of red, green, and blue components of a color image in order to create a false color composite (FCC). Digital elevation data from the ALOS mission with a resolution of 1 arc-second (~30 m) were used as base data to create a DEM mosaic of the study area as well as shaded relief and slope maps. All sinks within the DEM data set were removed to produce a DEM without depressions avoiding possible discontinuous drainage networks in the following processing steps. Flow direction and flow accumulation were then derived and a stream network was delineated. In addition, drainage divides in the surroundings of the Ramgarh structure were determined by combining the derived flow direction with defined outlet points.

Faults were mapped by a combination of field analysis that includes the measurement of attitude of strata on both sides of the faults, and remote sensing analysis of lineaments using flexible color stretches of DEMs and BaseMap imagery. Orientations of faults and strata were analyzed segmentally by means of their "concentric deviation" with respect to the center of the structure applying the technique described in Poelchau and Kenkmann (2008). In addition, gravity disturbances were analyzed using GGMplus data (Global Gravity Model plus, Hirt et al. 2013).

GEOMORPHOLOGY

Ramgarh is situated close to the eastern border between Rajasthan and Madhya Pradesh, some 110 km northeast of the city of Kota and 350 km SSW of Delhi. The name-giving village of Ramgarh is immediately south of the structure (Fig. 1C). Access to the structure is via the towns of Baran (28 km SW of the structure center) and Mangrol (11 km west of the structure's center).

Ramgarh is a 200 m high topographic landmark in otherwise flat terrain of intense agricultural use (Figs. 1, 2, and 3C). The Parvati River runs from south to north and approximates the western part of the annular topographic structure by approximately 4 km (Figs. 1B, 1C, and 2A). The present course of the Parvati River to the west of the Ramgarh structure is irregular compared to the rest of the course of this river (Misra et al. 2019). The tributary Kul River lies east of the annular ring and confluences with the Parvati River approximately 7 km NNW of the center of the structure (Fig. 1C). Approximately 3 km upstream of this confluence, an unnamed larger tributary discharges into the Kul River. This tributary partly delineates the crater outline as will be detailed later. River beds are incised into the plain by some 15–20 m and partly expose consolidated bedrock beneath a thick cover of unconsolidated Quaternary alluvial sand, silts, and soil.

The topographic collar has a crest-to-crest diameter between 2.2 and 2.7 km, with the largest diameter in NNE–SSW direction (Fig. 2). The diameter of the annular feature, measured from its outer limits at the base of the outer slope, is 3.5–4.0 km, with the largest diameter again in NNE–SSW direction. The collar

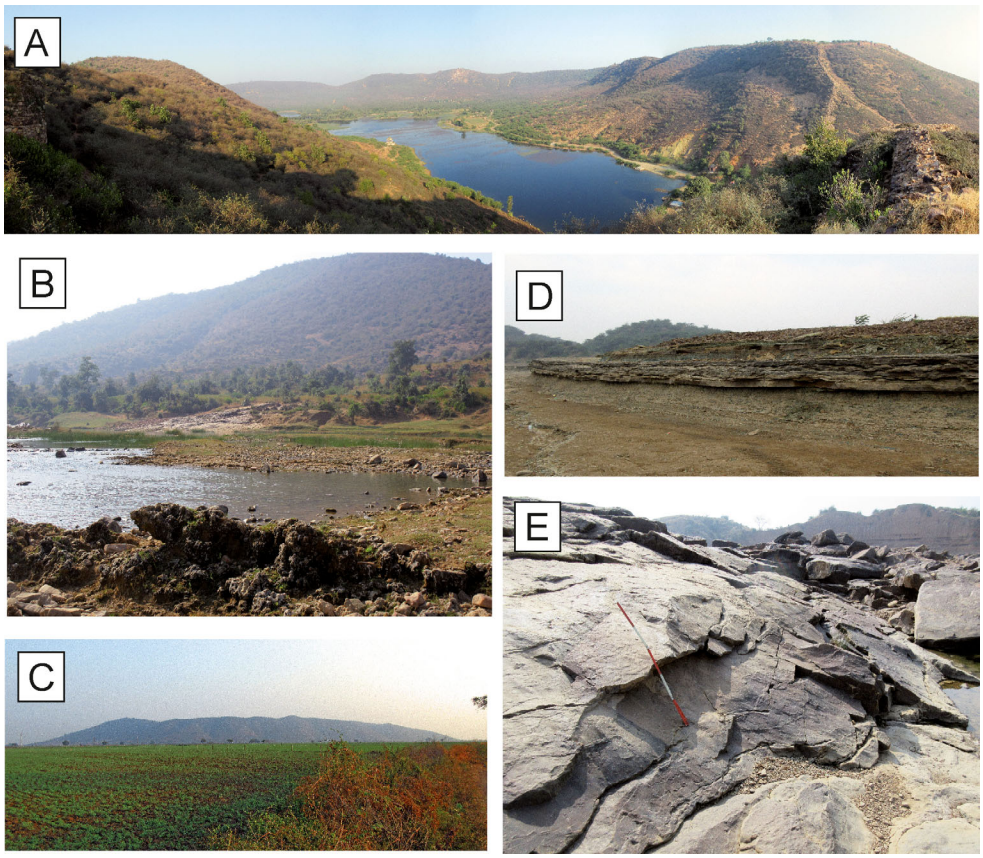

Fig. 3. A) Panorama view from the SW collar showing the central uplift and its southwestern outlet with dammed lakes. The center of the crater is behind the far end of the lake. Exposure of Shamria Shale is close to the shore of the near-end of the lake. B) View toward the SW view over the Kul River toward the collar of Ramgarh. In the foreground, tilted and cemented beds of diamictite are exposed. C) View from the north toward the Ramgarh collar and its surrounding flat plain. At its base, the collar is 3.5–4 km wide. D) Large exposure of flat-lying thinly bedded Sirbu Shale along the Parvati River bed, west of the Ramgarh structure. E) Exposure of the crater rim fault in the Kul River bed, south of the Ramgarh annular collar. The fault plane strikes concentrically and dips with 30°–35° toward the center of the structure. Note the striations on the fault plane (1 m stick for scale). (Color figure can be viewed at wileyonlinelibrary.com.) (Color figure can be viewed at wileyonlinelibrary.com.)

deviates from circularity and has a somewhat rectangular shape with rounded corners (Fig. 2). The inner slopes of the collar are steeper than the outer flanks. The outer slopes are inclined by 20°–30°, whereas the upper parts of the inner slopes have steeper dips of 30°–40° (Fig. 2C). The width of the annular ridges of the collar measured in radial directions varies from 0.8 to 1.3 km. The collar is remarkably continuous, breached only in the southwest by the outlet of the central depression (Figs. 2 and 3A). The inner depression hosts a swampy area with two lakes in the SW sector that are artificially dammed against the outlet in the SW. Generally, the inner depression is slightly elevated against the surrounding plain (Fig. 2B). The datum of the larger lake is approximately 10 m above the elevation of the plain surrounding the annular feature.

LITHOLOGIES AND STRATIGRAPHY

The structure is situated in the center of the Proterozoic Vindhyan Basin (Bose et al. 2001). The Vindhyan Basin is located on the Bundelkhand Craton and wraps around Bundelkhand Granite (Ramakrishnan and Vaidyanadhan 2008). The basin, in turn, is superposed by the Deccan traps in the SW and by the Indo/Gangetic Alluvium in the North. Strata of the Vindhyan Basin are virtually undeformed and were not metamorphosed. They are subdivided into the Lower and Upper Vindhyan of the Vindhyan Supergroup. The Upper Vindhyan is subdivided into the Kaimur, Rewa, and Bhander Groups (Oldham 1856). At Ramgarh, strata of the Rewa and Bhander Groups are exposed. The Kaimur Group is a coarsening upward sequence of shales, siltstone, and sandstones, and was

only drilled at Ramgarh. The 100–300 m thick Rewa Group thickens toward the north and commonly shows lateral facies changes. It starts with basal reddish shale (Panna Shale) followed by limestone and so-called Asan Sandstone. The Lower Rewa Sandstone in the hanging wall is superposed by a conglomerate bed and the variegated Jhiri Shale. The upper sequence of the Rewa Group is dominated by partly poorly sorted, immature sandstones (Drummondganj Sandstone, Govindgarh Sandstone, Upper Rewa Sandstone). The Neoproterozoic Upper Rewa Sandstone represents the oldest stratum exposed in the structure (Fig. 4B).

In the context of the Ramgarh structure, the most important lithological package is the Bhander Group that reaches a thickness of 1300–1500 m along the axis of the Vindhyan Basin. The lowermost unit of the Bhander Group is the Ganurgarh Shale, which is a succession of shales, stromatolitic limestone, sandstone beds, and an intra-formational breccia with halite casts that is interpreted as a lagoonal tidal flat complex (Ramakrishnan and Vaidyanadhan 2008). The Ganurgarh Shale sequence is topped by the Lower Bhander Limestone. It comprises algal mats, stromatolitic limestone, and gypsum layers formed in a tidal flat lagoonal facies. In the area of Ramgarh follows a sequence of red and green claystone, named Shamria Shale. This sequence is superposed by the Lower Bhander Sandstone of the Bhander Group that represents a thick fining-upward sequence of mainly red-colored sandstones with heavy mineral layers formed most likely in a tidal flat environment as a barrier beach. This fining upward sequence eventually grades into purple and green shale deposits, called Sirbu Shale. The stratum contains casts of halite and gypsum,

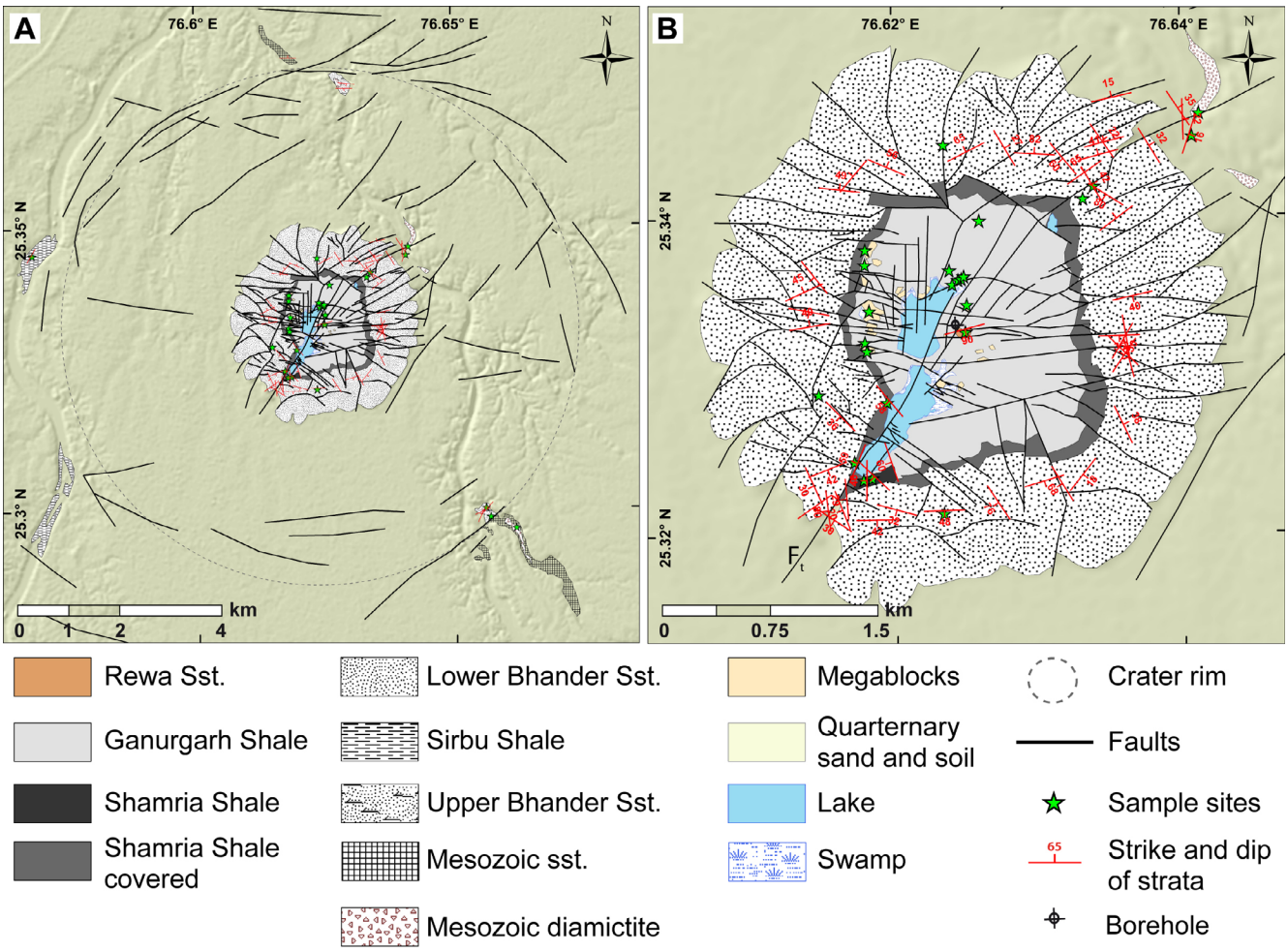

Fig. 4. Geological map of the Ramgarh structure (A) including a detailed view of the annular collar (B; map units superposed on ALOS shaded relief). (Color figure can be viewed at wileyonlinelibrary.com.) (Color figure can be viewed at wileyonlinelibrary.com.)

and was obviously deposited under arid conditions with high evapotranspiration. The final lithological unit of the Bhander Group is the Upper Bhander Sandstone. The Upper Bhander Sandstone shows ripple marks, cross bedding, and marly limestone beds, and is intercalated with stromatolitic limestone beds. A near-shore littoral paleo-environment is suggested with sandstone being formed in a fluvial to deltaic environment and admixture of eolian sandstones (Ramakrishnan and Vaidyanadhan 2008). The Upper Bhander Sandstone, constituting the youngest formation of the Vindhyan Supergroup, has been radiometrically dated as 1000–1070 Myr using U-Pb detrital zircon ages (Malone et al. 2008). In our mapping campaign at Ramgarh, we have used the aforementioned lithostratigraphic units of the Rewa and Bhander groups (e.g., Ramasamy 1988).

In the area surrounding Ramgarh, the strata of the Vindhyan Supergroup, forming the Kota Plateau, are mostly flat-lying and the exposure in the central part of the basin is of Bhander Group rocks (Prasad 1984). Toward the margin of the basin, lower strata become exposed. Sirbu Shale was mapped in the plains surrounding the Ramgarh structure, in the south, west, and north, whereas Lower Bhander Sandstone is exposed to the east (Rakshit 1973), indicating a very gentle dipping of strata in the order of 1°–2° toward the west. Within the domal structure of Ramgarh, deeper stratigraphic units are exposed.

Strata of the Collar and the Central Depression

The central depression is covered by soil (Fig. 4B). A 452 m deep bore hole drilled in 1981–1982 by the Geological Survey of India (Ramasamy 1988) into the center of the structure through the thick layer of soil revealed the underlying sequence. It started at the top with Ganugarh Shale and followed by other underlying shales, siltstone, and sandstones belonging to the Rewa and Kaimur Groups of the Upper Vindhyans, which are uplifted by approximately 1 km (Ramasamy 1988). The log description of this borehole, drilled in 1981–1982, is unfortunately not accessible.

The oldest stratum exposed within the center of the domal structure is Upper Rewa Sandstone (Fig. 4B), a beige, relatively pure, quartz-cemented sandstone that shows intense cataclasis and deformation. It forms a small hill, approximately 6 m high and 20 m wide at the base, close to the geographic center of the structure and next to an old Hindu temple. The next younger unit is the Ganugarh Shale Formation that comprises shales, sandstones, as well as limestones. The rarely exposed Lower Bhander Limestone in the hanging wall of the Ganugarh Shale forms a few meter thick band along the periphery of the central depression and has been mapped together with the Ganugarh Shale Formation (Fig. 4B). Buff-colored, strongly competent quartzitic sandstones exposed in the western part of the depression are dissimilar to the rocks building the collar. They form a hummocky terrain in the foothills of the western collar and are interpreted as megablocks (Fig. 4B). Their stratigraphic provenance is not clear. From their spatial position, they could represent silicified sandstones from the Ganugarh Shale Formation. However, they could also represent Upper Rewa Sandstone.

The next stratigraphic unit in the hanging wall is the green and red Shamria Shales of the Bhander Group that are well exposed close to the outlet of the central depression at the inner slope of the annular collar (Figs. 3A and 4B). However, the lower parts of the inner slopes of the collar are largely covered with alluvial fans and talus. Talus material is primarily Lower Bhander Sandstone. The pronounced collar is formed by competent, red, hematite-bearing Lower Bhander Sandstone that has an estimated thickness of approximately 200 m (Figs. 3A and 4B). The sandstone forms thick quartzitic beds and shows internal cross stratification. Minor feldspar, tourmaline, and zircon are present as accessory phases.

Strata Exposed in the Area Surrounding the Collar

Around the collar, Sirbu Shale is exposed at two locations along the Parvati River bed; one of them is labeled E in Fig. 1C (Fig. 4A). Here occurs a succession of thin siltstone and claystone beds of alternating reddish and greenish color interbedded with thin sandstone layers and gypsum interbeds with halite casts (Figs. 3D and 4A). The fine-grained beds show mudcracks. The strata show regionally very gentle warping and lie subhorizontally with maximum dips of approximately 4° (Fig. 5).

A different stratigraphic succession is exposed along the tributary Kul River at locations B (Fig. 1C) in the northern part of the structure and at D (Fig. 1C) in the southern part of the structure (Fig. 4A). Due to tilting of the strata, a roughly 25 m thick section is exposed at B and 45 m at D (Figs. 4A, 6 and 7A). This section shows—from the footwall to the hanging wall—a sequence of interbedded marly limestone, disintegrated limestone with intra-formational slabs (Fig. 7B), siltstone and sandstone layers with conglomeratic beds (Fig. 7C), limestones with abundant subrounded intraclasts (Fig. 7D), and strongly weathered and variegated horizons with gypsum layers. The section ends with a 10 m thick layer of stromatolitic limestone (Fig. 7E). The sequences at locations B and D are very similar and represent the same stratigraphic horizon. As

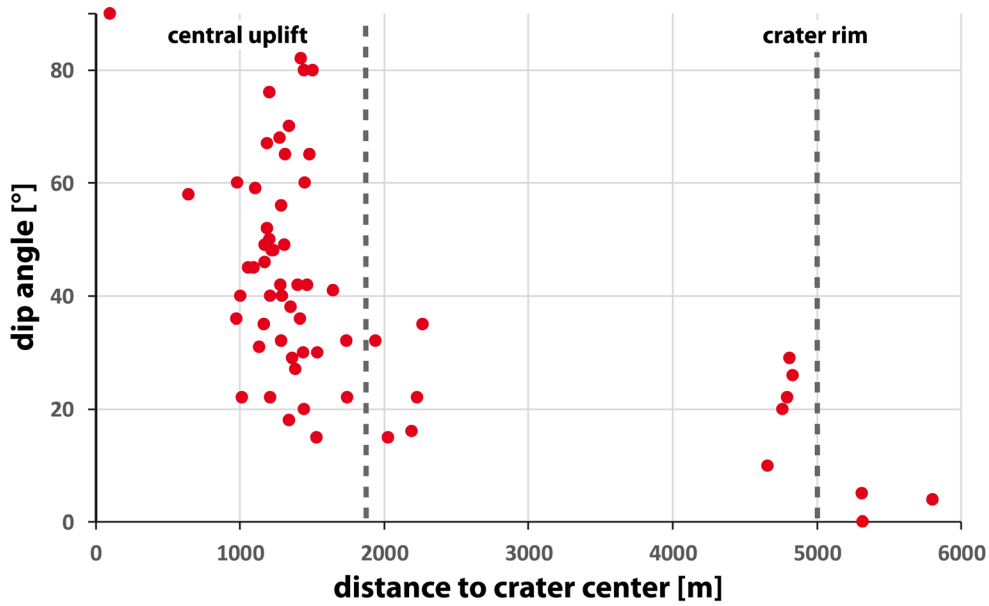

Fig. 5. Dip data of strata as a function of their radial distance from the crater center. (Color figure can be viewed at wileyonline library.com.) (Color figure can be viewed at wileyonlinelibrary.com.)

the entire sequence is uniformly tilted, it must have been a consolidated sequence at the time of tilting. The sequence represents the Upper Bhander Sandstone formation that is known for its stromatolite layers. However, sandstones are of subordinate importance in this sequence.

Adjoining the locations B and D are the outcrops A and C, respectively (Fig. 1C), at increasing distance

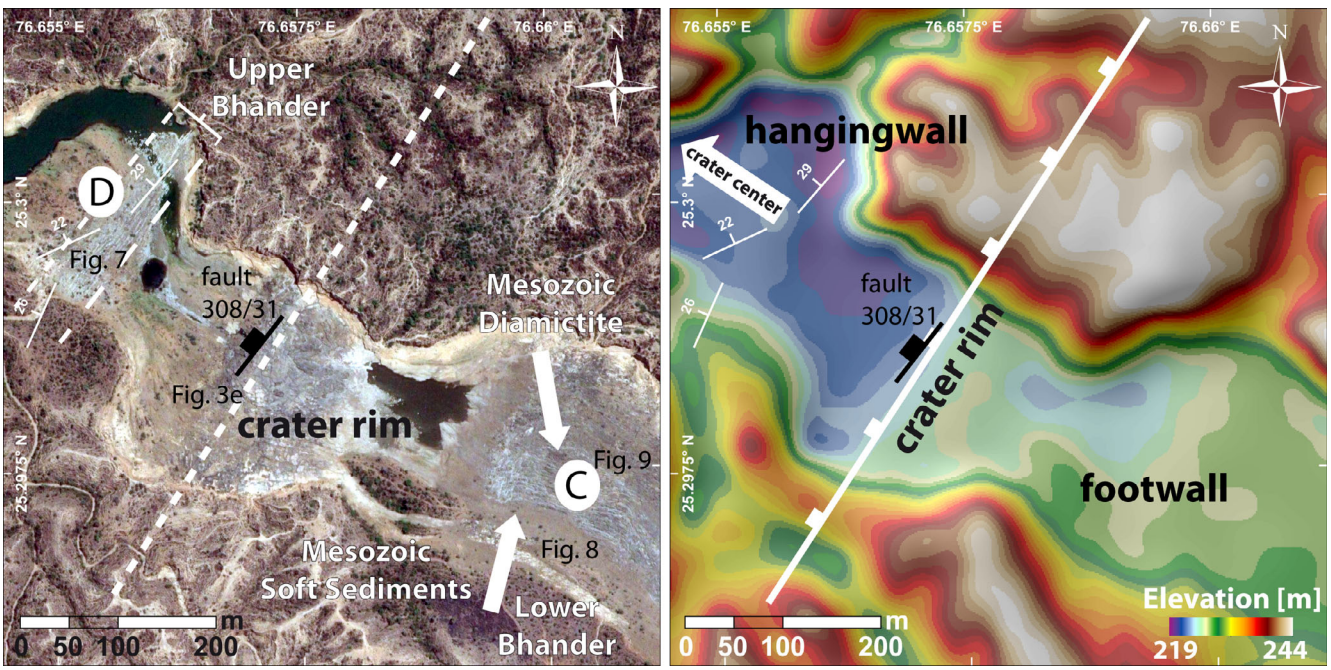

Fig. 6. Close-up view of the southern crater rim area with the locations C and D (Fig. 1C) of the Ramgarh structure based on Digital Globe imagery (left) and ALOS-DEM (right). The crater rim fault crosses the river bed and forms a topographic step. Note that the hangingwall strata at location D dip concentrically toward the crater center, whereas the footwall strata at C are flat-lying. (Color figure can be viewed at wileyonlinelibrary.com.)

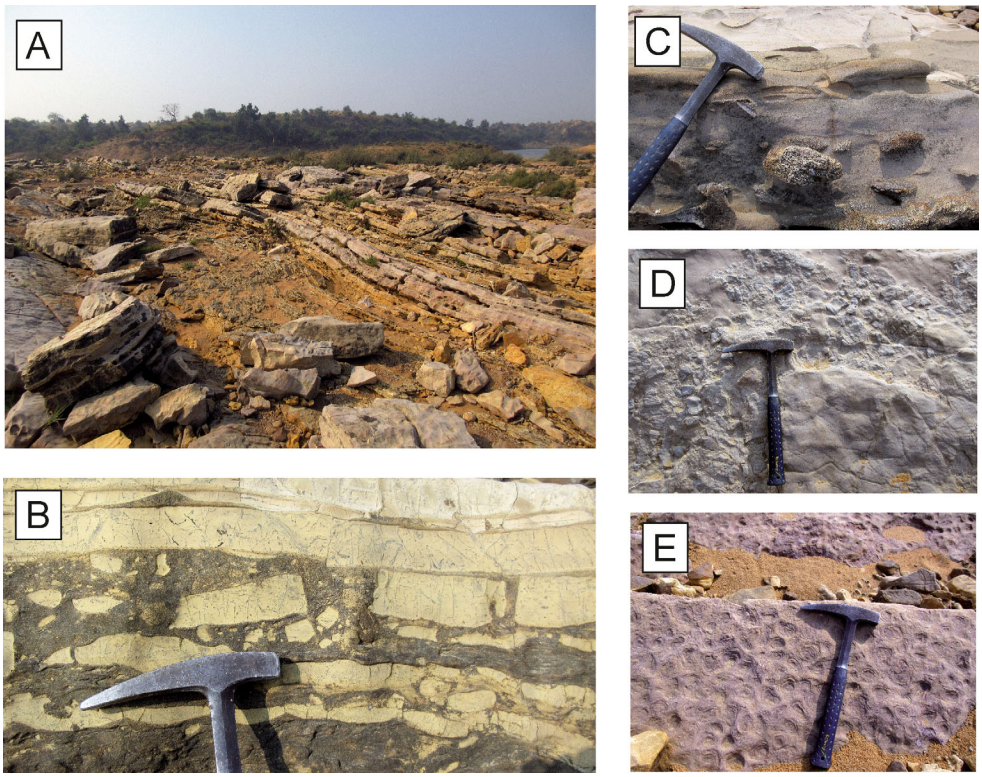

Fig. 7. A) Overview of location D (see Fig. 1C) inside the southern crater rim at the river bed of the Kul River. Strata composed of limestone, sandstone, and conglomerate are coherently tilted by 25° toward the NNW. Figures (B–E) are from this sequence. B) Marly limestone beds are disintegrated into slabs surrounded by a fine-grained matrix. C) Sandstone bed with subrounded pebbles and boulders. D) Limestone with abundant intraclasts. E) Stromatolitic limestone is the youngest and final deposit of this exposed tilted sequence. (Color figure can be viewed at wileyonlinelibrary.com.) (Color figure can be viewed at wileyonlinelibrary.com.)

from the collar of the Ramgarh structure. These outcrops are quite large and comprise the entire river bed (Fig. 6). They expose beige sandstones with large cross-beds and were mapped as Lower Bhander Sandstone by Rakshit (1973). A remarkable difference to B and D is that the strata here are flat lying (Fig. 8A). Both locations A and C present in their upper parts strong and impressive evidence of soft sediment deformation. The sandstones show intricate meter-scale folds with various orientations and hinge thickening (Figs. 8D and 8E). Recumbent folds (Fig. 8D) and other folds with upright fold axial planes occur in close proximity of each other. Fold interference leads to small-scale dome and basin structures (Figs. 8B and 8C). The local limb attitudes vary from horizontal to upright, and even overturned, within meters. This folded upper unit, which is locally intermingled with conglomerates and diamictite of the superposed layer (Figs. 8E and 9C), indicates that the overlying diamictite layer and the sandstone that show soft sediment deformation were deposited simultaneously.

Diamictites occur widespread at location C and are exposed with 2–3 m thickness. Near the contact to the underlying sandstones, the diamictites comprise angular to subrounded slabs of limestone, sandstone, and other lithologies of 20 cm up to meter size (Fig. 9A). Slabs and elongated clasts show an alignment and shape-preferred orientation, with their flat side oriented subhorizontally. In a fining upward sequence, clasts become more rounded and smaller in diameter. Still, grain size sorting is poor and grain sizes vary between blocks of several decimeter and pebbles of a few millimeters in size (Fig. 9B). The diamictites are always consolidated by a competent grayish matrix of mostly sand-sized particles and carbonate, as well as silica-rich cement. Clasts and particles include well-rounded, reddish-purple sandstones, beige sandstones, and pale carbonates, to only name the most abundant lithologies. The diamictites contain abundant gastropod fossils (Figs. 9D–F). They are cemented in the matrix of the diamictite and show sparitic calcite replacement of the shell. The specimens are small- to medium-sized (12–24 mm height, 10–13 mm diameter) littoriniform shells with convex whorls. According to the taxonomic characterization of the specimens (Table 1), the

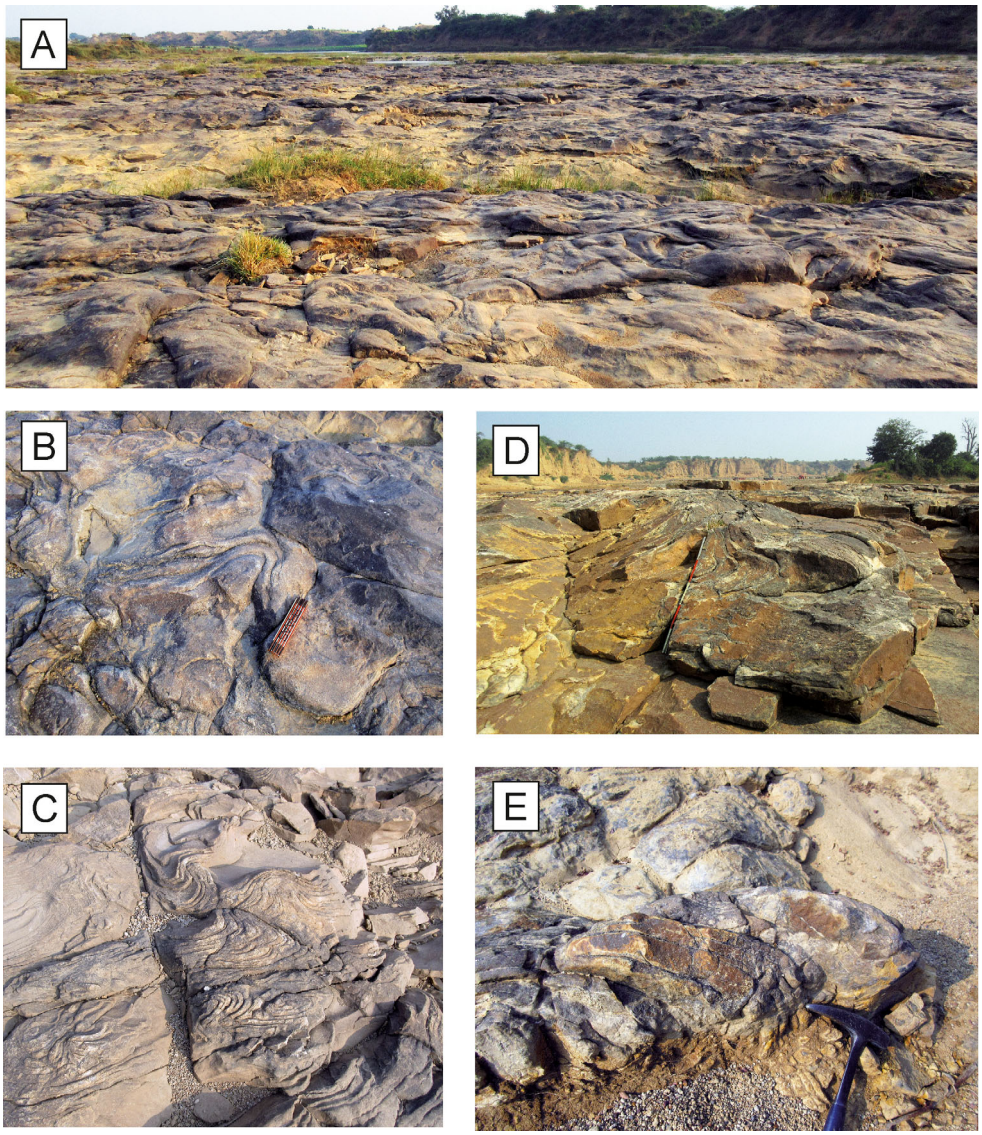

Fig. 8. A) Location A outcrop (see Fig. 1C) just outside the crater in the Kul River bed. Sandstone strata are flat-lying but show intense convolute bedding. B) Convolute bedding with dome and basin structures on the decimeter-scale (folding yardstick, 25 cm, for scale) (Location A). C) Disharmonic folding without fracturing indicates soft sediment deformation of sand under high fluid pressure. The granular sand was later solidified to sandstone (image width ~1 m; Location A). D) Meter-scale recumbent fold with strongly thickened fold hinge (1 m stick for scale) (Location C). E) Recumbent sand fold with thickened fold hinge and entrained pebbles of the overlying conglomerate (Location C). (Color figure can be viewed at wileyonlinelibrary.com.) (Color figure can be viewed at wileyonlinelibrary.com.)

gastropods belong to the family *Ampullinidae Cossmann 1918*. The genus *Ampullospira sp. Harris 1897* found in the Amphiastrea Bed of the Washtawa Dome of western Rajasthan agrees well with our measurements, but the gastropods of the diamictite bed are slightly smaller than those reported in Alberti et al. (2013) and may represent juvenile specimens. Smaller specimens of similar habit belonging to the same family are of the Genus *Omphaloptycha Kittl 1894*, though these specimens have more flattish to slightly convex whorls. Both specimens have an Upper Middle Jurassic age, of 165 ± 1.3 Myr (Alberti et al. 2013).

STRUCTURE

Macro-Scale Deformation

The striking morphological landmark of Ramgarh is the annular collar that is the remnant of a domal

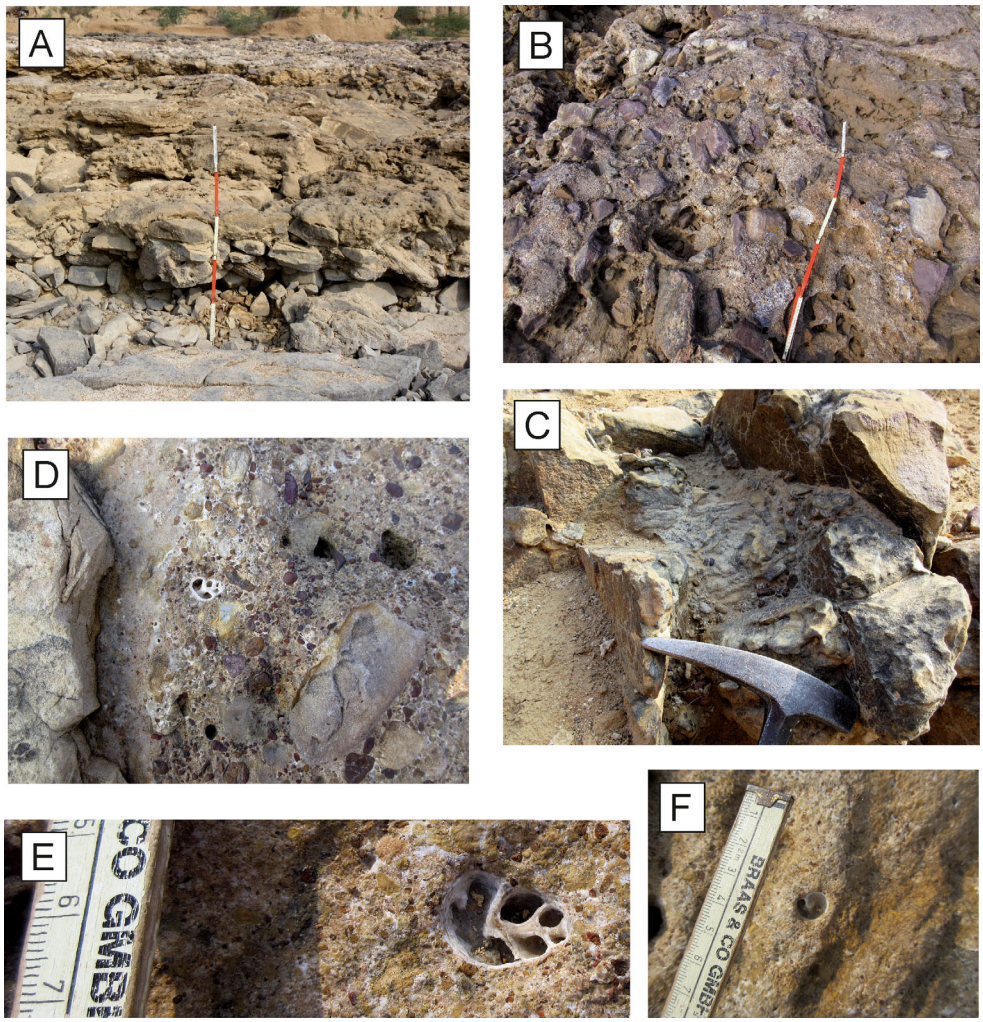

Fig. 9. A) Location C (Fig. 1C) south of the southeastern rim fault. The basal diamictite in contact to the underlying reworked sandstone shows up to a meter-sized angular blocks of limestone and sandstone and is well cemented, but also displays open pore space (1 m stick for scale). B) Subrounded clasts up to 30 cm in diameter are cemented in a grayish matrix of small pebbles and sand-sized particles (1 m stick for scale). C) Transition between the underlying sandstone and diamictite bed. Both lithologies are tightly interlocked and indicate deposition in the same event. Note that the interface between the convolute sandstone and the diamictite is vertical. D) Sections of gastropod shells can be commonly observed in the well-cemented matrix of the diamictite beds. The shells are replaced by sparitic calcite. (image width is 25 cm). E) We identified juvenile forms of the genus *Ampullospira sp. Harris 1897*. F) Section perpendicular to the gastropod spire axis. (Color figure can be viewed at wile yonlinelibrary.com.) (Color figure can be viewed at wileyonlinelibrary.com.)

Table 1. Morphological characteristics of gastropods cemented in diamictites of location C of Fig. 1C.

Morphology	Value	Error
H [mm]	18	5
HL [mm]	9	1
HP [mm]	10	2
D [mm]	12	2
α [°]	46	7

H: height; HL: height of last whorl; HP: height of peristom; D: diameter; α: mean spire angle.

uplift (Figs. 1, 2 and 3A). Previous studies have emphasized the domal structure with concentric strike of strata and outward directed dips. The inner part of the uplift shows a relief inversion, that is, the center of the uplifted structure presently forms a more or less circular topographic depression. On the one hand, this inversion may be due to the dominance of incompetent claystone (Ganugarh Shale) in the center (Fig. 4B), whereas the periphery is formed by competent sandstone forming the collar. On the other hand, it be caused by an increase in cataclasis toward the center

(Fig. 11). Our structural analysis of the collar shows two important characteristics: first, the collar is dissected by numerous faults that show sectoral characteristic arrangements with preferred radial, concentric, or oblique strike (Fig. 4B), and second, bedding planes show prominent and systematic deviations from concentric strike (Fig. 4B).

The collar is discontinuous in the southwestern sector, where the outlet valley from the central depression is formed (Figs. 1, 2, and 2A). A steeply dipping, NE–SW trending, dextral strike-slip fault (Misra et al. 2008, 2019) with a shear displacement of approximately 400 m can be deduced from the off-set of the strata in the collar. The fault crosses the center of the structure, bends by 10°–20° toward the east, and truncates the northeastern collar, and can be traced outside the collar where it crosses the Kul River. This major fault is denoted as F_t in Fig. 4B. The southwestern sector of the collar on both sides of F_t is characterized by several broadly NW–SE striking reverse faults that cause intraformational repetitions of the Lower Bhander Sandstone and enlarge the width of the collar in this area. From the apparent curved outcrop trace of these faults, a fault dip to the SW is indicated. The second set of faults trends parallel to F_t, and has an average spacing of 450 m. On the opposite side, in the NE sector, faults perpendicular to F_t are missing. Instead, a NE to ENE trending fault swarm, slightly divergent, dominates, and has a more or less radial character with respect to the structure's center (Fig. 10). The dextral offset of F_t is less obvious here than in the SW sector and seems to be distributed over the entire fault swarm. Faults are closely spaced with an average spacing of only 200 m. Faults in the NW and SE sectors are neither concentric nor radial. Some of the faults identified by us were also mapped by Ramasamy (1987) and Misra et al. (2019). Faulting intensity increases toward the center of the structure. Remote sensing analysis allowed partial mapping of the fault lineaments within the depression, even though large areas are covered by soil. In the western part of the depression, it is possible to partly reconstruct a network of intersecting faults trending both subparallel and perpendicular to F_t. As a consequence of fault

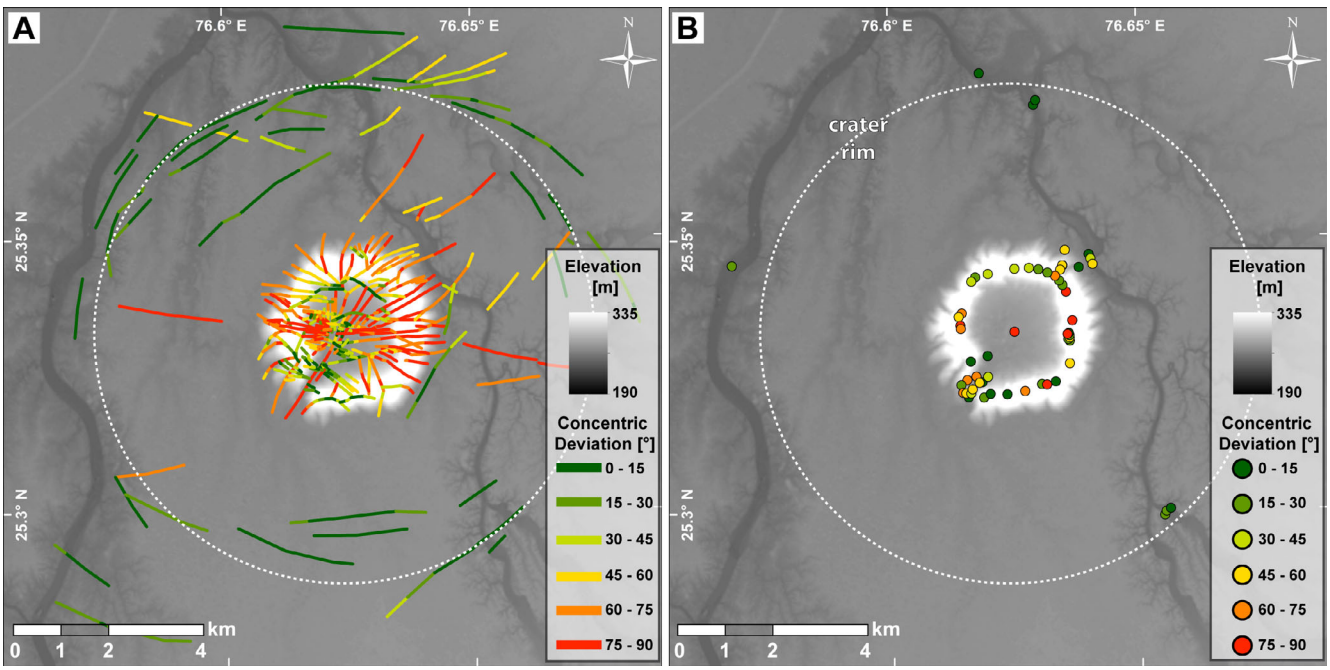

Fig. 10. Map showing the concentric deviations of faults (A) and bedding strikes (B; superposed on ALOS DEM). A) Near the crater rim, the strata show no or minor concentric deviation. Along the collar, the concentric deviation is high in the crossrange sectors (SE and NW) and low in the uprange (SW) and downrange (NE) sectors. Deviations from concentric strike in these sectors occur where the bedding is dragged close to faults, in particular the main SW–NE fault. B) The mapped faults and lineaments were analyzed in 200 m long segments with respect to their concentric deviation. The crater rim at 5 km radius is well expressed by concentric lineaments in the W, N, and E sectors, but has a faint expression in the southern part. The E–W trending lineament crossing the collar can also be traced outside the structure and is interpreted as a feature of later regional tectonic origin. Radial lineaments are particularly common in the downrange sector (NE). Within the collar, concentric faults dominate in the SW (uprange) sector, whereas radial and oblique faults characterize the other parts of the collar.

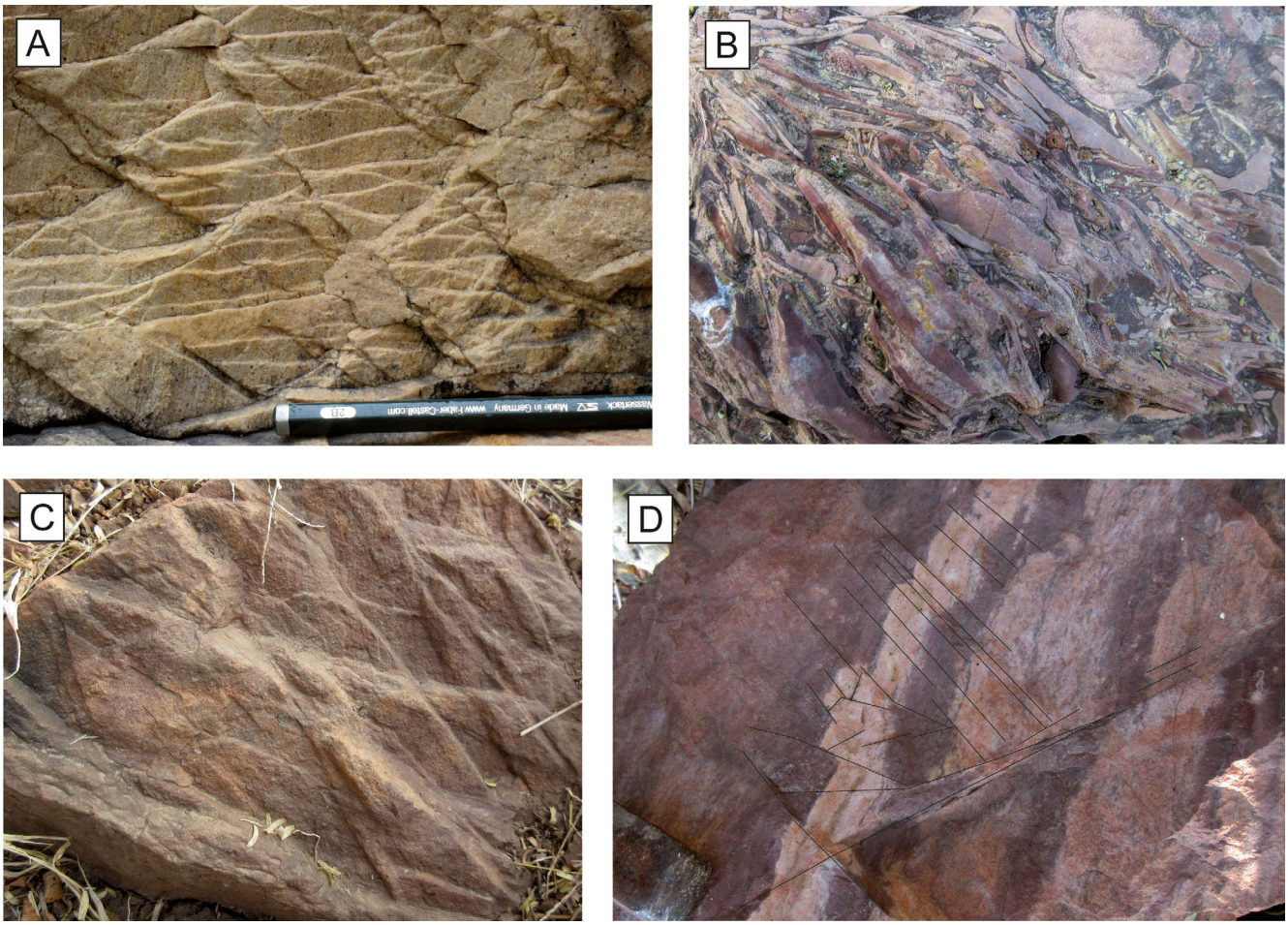

Fig. 11. A) Rewa Sandstone from the center of the structure. Narrow-spaced faults intersect each other and cause stair-stepping displacements of the vertical bedding planes. This arrangement is known from the central uplift of other craters (10 cm pencil for scale). B) Red siltstone of the Ganurgarh Shale formation is disintegrated into centimeter-to-decimeter-sized flakes that are embedded into a sandstone matrix (image width 20 cm). C) Network of small-scale faults in Lower Bhander Sandstone of the collar. Oblique fault intersections produce apical structures. These are not shatter cones! Shatter cones have not been found at Ramgarh so far (image width 20 cm). D) Variegated Lower Bhander Sandstone shows an array of centimeter-spaced, parallel faults with small displacements. (Faults have been marked for easier recognition. Image width 25 cm.)

intersection, elongated mega blocks with widths ranging from a few decameters to approximately 100 m have become isolated. The blocky nature is also evident topographically from a hummocky relief.

The finding of all previous studies (except Misra et al. 2019) that strata strike concentrically and quaquaversal at the collar with respect to the structure's center is an oversimplification and only holds true for the outer periphery of the collar. The deviation from concentric strike is locally very strong and shows some systematic trends (Figs. 4B and 10). The strike commonly changes abruptly in narrow zones across the mapped faults (Fig. 4B), indicating block rotation during uplift. At proximity to the faults, strata may be subparallel to the faults, due to dragging of beds along the fault planes and local rotation of rock slices in the damage zones of the faults. This is, for instance, the case near the major fault F_t close to the valley outlet and in the NE sector of the collar. Otherwise, strata show weak concentric deviations in the SW and NE sectors. This is in contrast to the NW and SE sectors where larger concentric deviations of beds were measured. Some of the bedding planes strike sub parallel to the oblique faults, whereas others are oriented oblique to the faults. This is in accordance with the statistical data for bedding planes by Misra et al. (2019) that also show a larger scatter and large concentric deviation in the SE and NW sectors. Figure 11 displays the dip angles with radial distance from the crater center. Dip angles between 20° and 60°

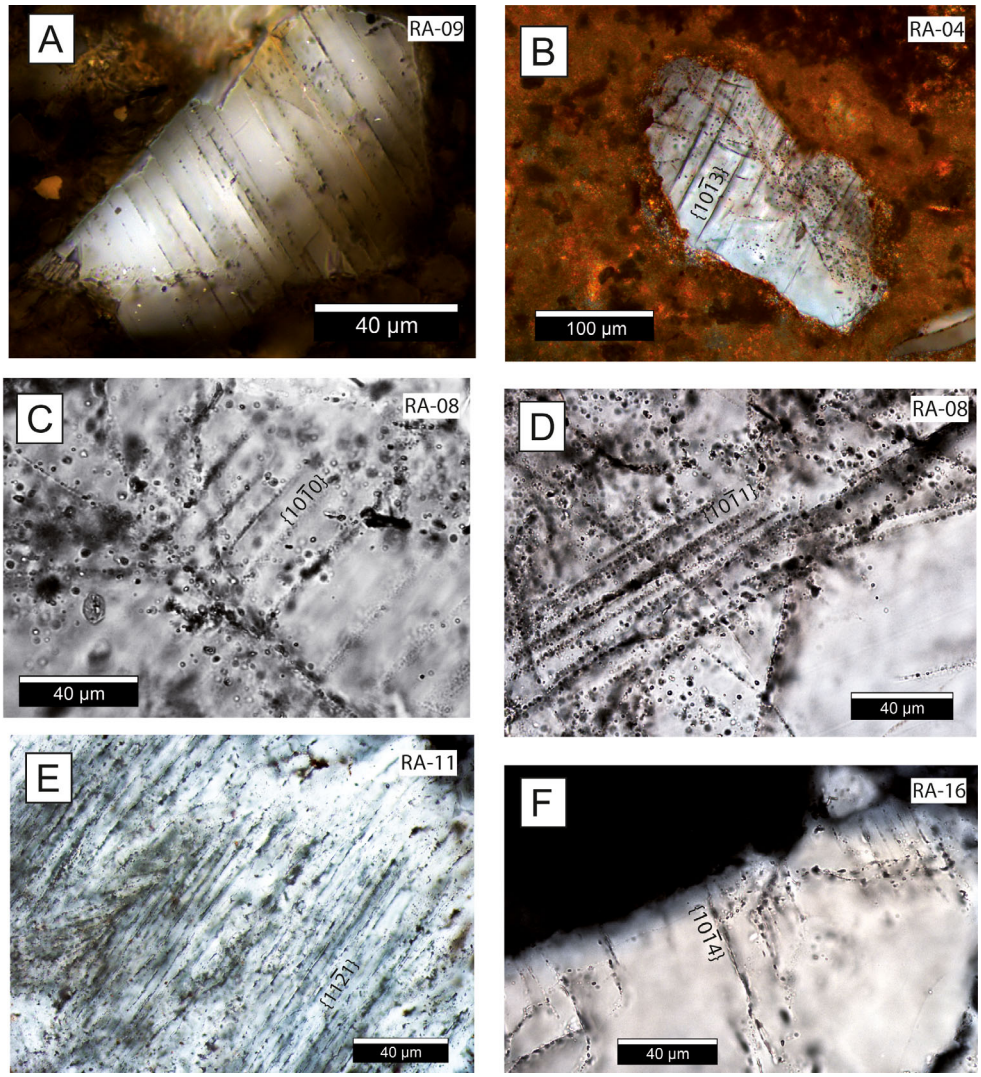

Fig. 12. The photomicrographs display quartz grains under crossed polarizers. All planar microstructures are decorated with fluid inclusions or opaque phases. A) PDF lamellae of breccia sample RA-09 have an average spacing of 2 µm. B) Quartz grain with long PFs crosscutting the entire grain. The grain is embedded in the fine-grained clastic breccia matrix of sample RA-04 that contains abundant iron oxides. C–D) Decorated PF lamellae in sandstone sample RA-08. E) Parallel set of lamellae with 3 µm average spacing in quartz grain of sandstone sample RA-11. The spacing suggests that the lamellae represent PDFs. F) Parallel lamellae at a quartz grain margin of sample RA-16 show a local spacing of 3-4 µm and are arguably interpreted as PDFs. (Color figure can be viewed at wileyonlinelibrary.com.) (Color figure can be viewed at wileyonlinelibrary.com.)

along the crest of the collar are common, but locally even overturned beds are observed, for example, at the Shiva temple along the eastern crest of the collar. The dips along the outer foothill of the collar are more gentle than along the crest of the collar (Fig. 5).

The very limited occurrence of outcrops in the central depression did not allow systematic measurement of the bedding attitude. The only exception is the little outcrop of strongly deformed Rewa Sandstone where the strata are oriented vertical and strike E-W to SE-NW.

Outside the collar, there are only few locations along the bed of the Parvati River and, in particular, along the Kul River, that allow structural measurements to be recorded. The two northern locations along the Kul River, labeled A and B in Fig. 1C, show a remarkable difference. The northernmost outcrop A shows flat-lying strata over a large exposure of the river bed with warping of strata on the meter scale (Fig. 8A). In contrast, at B, the strata dip consistently 10°–20° southward toward the collar, with perfectly concentric strike. The southern outcrops C and D (Figs. 1C and 6) along the Kul River

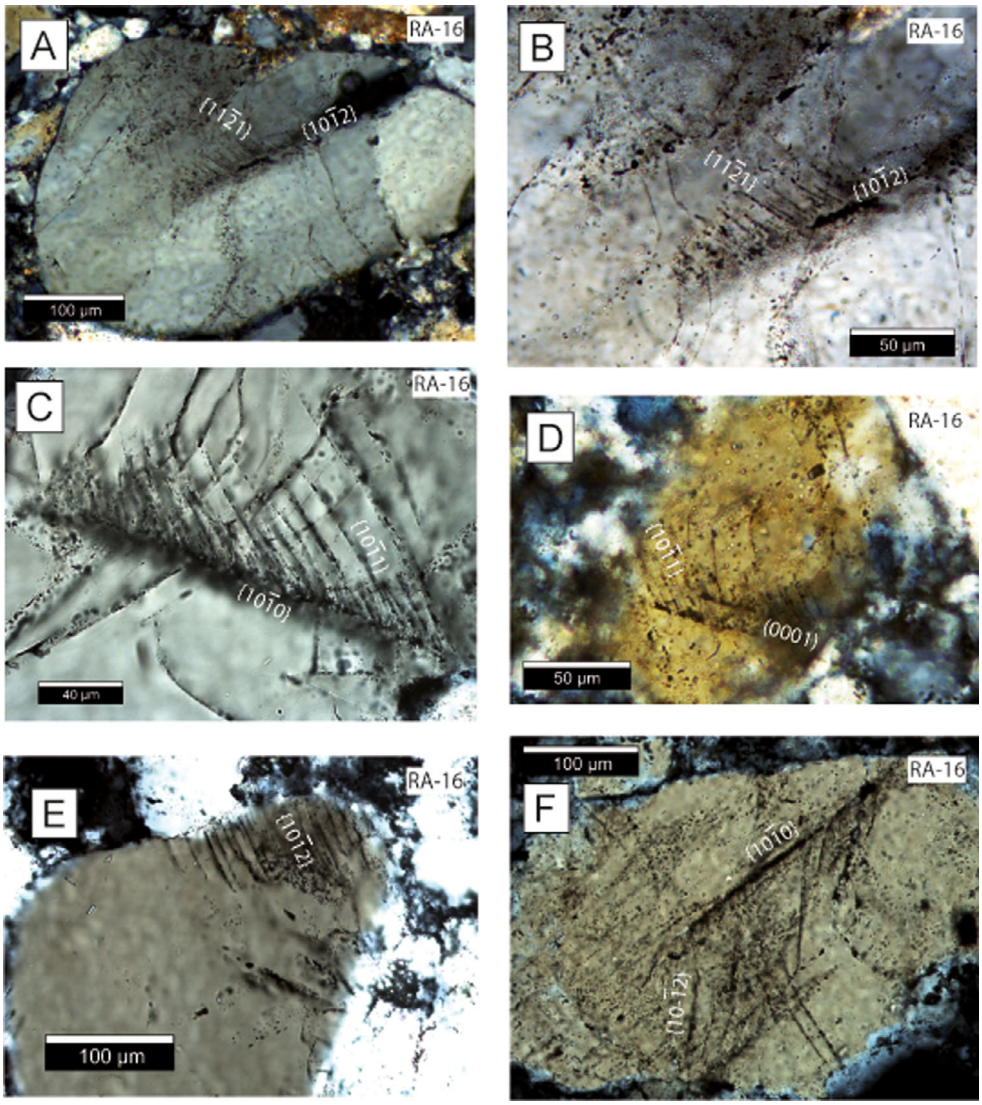

Fig. 13. Photomicrographs from sample RA-16 show quartz grains under crossed polarizers. All planar microstructures are decorated with fluid inclusions or opaque phases. A) Two parallel PF–FF sets developed in a rounded quartz grain where the crystal lattice is strained as indicated by undulose extinction. B) Close-up of (A): The parallel set of crystallographically controlled FFs have an average spacing of 4 µm. C) Set of a PF with long FFs. Note that FF lamellae are typically straight and parallel close to their base at the PF but can become increasingly curved with progressive length. The crystallographic control of FF lamellae is strong near the PF. With increasing distance, they can transform and propagate as standard fractures (Poelchau and Kenkmann 2011). D) Two PF lamellae from which FFs emanate. E) PFs near the margin of a quartz grain, with average spacing of 7 µm. F) Set of long PF lamellae from which FFs emanate. (Color figure can be viewed at wileyonlinelibrary.com.) (Color figure can be viewed at wileyonlinelibrary.com.)

show a similar structural situation. In the south, at C, a very large exposure of flat lying strata shows strong warping on the decimeter to meter-scale due to soft sediment deformation. However, further north at D, across a large normal fault of concentric strike (Figs. 3E and 6), the strata dip up to 30° toward the collar with nearly perfect concentric strike (Fig. 7A). The transition from A to B and from C to D defines the rim of the structure as marked by a normal fault. The normal fault between C and D is very well exposed where it crosses the entire river bed (Figs. 3E and 6). It is a low-angle normal fault with polished and striated surface that commonly merges into bedding planes, thereby forming a flat-and-ramp structure. The observed ramps typically have a fault dip angle ranging between 30° and 35°, whereas the flats are almost horizontal and parallel to bedding planes. The formation and slip on low-angle faults require unusually low friction coefficients along the fault planes and the presence of mechanically weak layers. The inward, toward the crater, dipping sediment sequences at

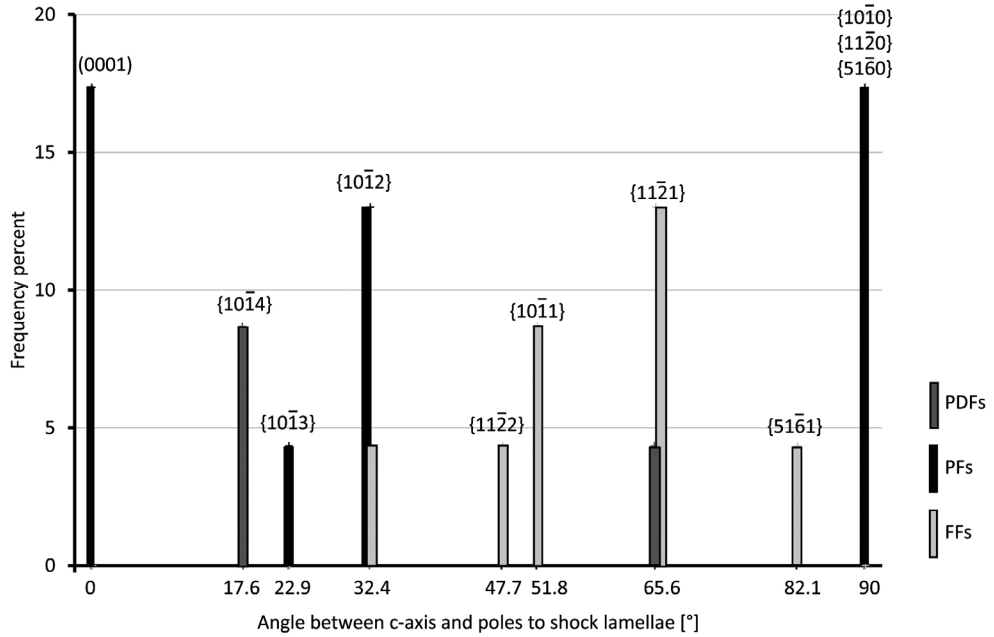

Fig. 14. Histogram of frequency percent of all 23 indexed PDFs, PFs, and FFs normalized to 100% in quartz grains. (Color figure can be viewed at wileyonlinelibrary.com.)

locations B and D are situated inside the crater rim faults and represent the hanging wall of the faults (see Fig. 15). The Lower Bhander Sandstone that forms the footwall of the crater rim fault at locations A and C is topped by sandstones that show soft sediment deformation and are topped with diamictites. In contrast, the exposed strata of the Sirbu Shale, west of the structure at the bed of the Parvati River (locality E, Fig. 1C), shows subhorizontal layering and is not disturbed.

Our remote-sensing analysis of lineaments outside of the collar shows distinct arcuate and concentric features at a distance of 4.8–5.5 km from the structure's center (Figs. 4A and 10). Such features are pronounced in the NW sector close to the eastern bank of the Parvati River. The curved lineaments can be traced to the abrupt kink in the Kul River channel (Figs. 1C and 4A). In the eastern sector, the channel of the eastern tributary of the Kul River flows north–south tracing the crater rim. The major fault F_t crossing the collar from SW to NE can be further traced to the NE where it crosses the Kul River, causing another sharp deflection of its course (Fig. 10A).

Another set of faint lineaments trending E–W across the collar can also be traced west and east of the structure. In agreement with Misra et al. (2019), this set of lineaments seems to be unrelated to the formation of the structure and appears to be the youngest deformation in the area that can be traced as regional lineaments well beyond the extent of the Ramgarh structure.

Meso-scale Deformation

Inside the domal structure, meso- and micro-deformation are ubiquitous. The shales in the borehole were partly isoclinally folded and are steeply dipping to subvertical in orientation (Ramasamy 1988). Rewa Sandstone, the oldest stratum exposed in the center of the circular depression (Fig. 4B), dips subvertically and shows pervasively faulted surfaces, each with a few millimeter average displacement (Fig. 11A). The fault spacing is on the order of less than 1 cm. This often results in a stair-stepping arrangement, a very common feature observed in many impact craters (Kenkmann et al. 2014). Inspection of the deformation inventory of the Ganurgarh Shale surrounding the central Rewa Sandstone relies on rubble stones and blocks that could be sampled along dry creek beds of the central depression. These rubble stones are angular to sub-rounded, up to several decimeter in size, and indicate short transportation distance. The maximum transport distance is constrained by the radius of the collar. We found claystone samples that show tight kink-folds, siltstone samples that are disintegrated into centimeter-sized flakes which are embedded into a dark sandstone matrix (Fig. 11B), and green, red, and gray-colored breccia float. Breccia sample RA-04 is polymict and contains centimeter-sized angular fragments of siltstone, reddish sandstone, and marly limestone embedded in a clastic matrix of finer grained fragments of the same lithologies. Breccia sample RA-09 is dark colored,

porous, and contains angular quartz clasts as well as irregularly shaped clasts of possible amorphous material that requires further microanalysis. In both samples, shock features could be identified (Figs. 12A and 12B). Float and rubble stones of monomictly brecciated sandstone, and sandstones with Fe-oxide impregnation, were also found in the center of the circular depression. Light-colored silicified sandstones are exposed at some of the little hummocks in the western part of the depression (Figs. 2A and 4C). These sandstones show intense meso- and micro-scale faulting but exhibit high competence due to later fracture sealing. The whitish color possibly indicates partial pulverization. Sample RA-16 taken from these rocks contains several shocked quartz grains (Fig. 13). The reddish Lower Bhander Sandstone forming the collar also shows narrow fault networks with offsets of a few millimeters to centimeters (Fig. 11D). The fault planes commonly meet in acute angles and cause structures that appear to have an apex and superficially resemble the shape of shatter cones (Fig. 11C). Three-dimensional analysis confirms that this structure is produced by intersecting slip planes and does not represent a shatter cone (Fig. 11C). In contrast, shatter cones have conical shapes with apices and are characterized by diverging and branching striae that lead to the so-called horse-tailing effect (e.g., Kenkmann et al. 2016). With increasing distance from the center, the frequency of narrow fault networks decreases. Misra et al. (2019) reported dominant fracture orientations parallel to the NE–SW, NW–SE, N–S, and E–W directions. These orientations largely correlate with the fault orientations shown in Fig. 4B. They also document that the fracture orientations differ from sector to sector.

Outside the domal structure, Sirbu Shale at location E does not show a particular deformation overprint. The tilted lithologies at locations B and D, tentatively classified as Upper Bhander Formation, display layers with intense deformation (Fig. 7). Among them are limestone strata with abundant angular intra clasts and brecciated horizons (Fig. 7D), limestones that are disintegrated into slabs at clayey interfaces (Fig. 7B), and beds with up to 70 cm-sized subrounded blocks of limestone. However, the indications of intense deformation are always stratiform and the entire sequence is homogenously tilted by 20°–30°. This suggests that the rock sequence was lithified and competent when tilting occurred. Therefore, a genetic link of the deformed lithologies at locations B and D to the Ramgarh deformation event seems unlikely though it cannot be completely ruled out.

The sandstones at locations A and C show intense soft sediment deformation. These rocks were in a weakly cemented to unconsolidated state when a forceful redeposition and mixing of the sands took place in the presence of water. Diamictites and conglomerates were emplaced on top of the sands. Their deposition occurred in the same event, as both lithologies are locally intermingled (Figs. 8E and 9C). Neither the sandstone nor the overlying diamictite show a brittle deformation overprint of the consolidated rocks.

Table 2. Shock features in quartz grains found at Ramgarh including sample name, location, and crystallographic orientation of shock lamellae.

Grain name	Sample	Figure	Latitude	Longitude	Shock feature	Orientation
Grain-1	RA-9	12A	25.33609° N	76.62469° E	PDF	
Grain-2	RA-4	12B	25.33573° N	76.62405° E	PF	PF1 - {10$\bar{1}$3}
Grain-3	RA-8	12C	25.33609° N	76.62469° E	PF	PF1 - {10$\bar{1}$0}
Grain-4	RA-8	12D	25.33609° N	76.62469° E	PF	PF1 - {10$\bar{1}$1}
Grain-5	RA-11	12E	25.33974° N	76.62591° E	PDF	PDF1- {11$\bar{2}$1}
Grain-6	RA-16	12F	25.33156° N	76.61814° E	PDF	PDF1- {10$\bar{1}$4}
Grain-7	RA-16	–	25.33156° N	76.61814° E	PF1 PF2	PF1 - {10$\bar{1}$2}, PF2 - {51$\bar{6}$1}
Grain-8	RA-16	–	25.33156° N	76.61814° E	PF, FF	PF1 - (0001), FF1 - {11$\bar{2}$1}
Grain-9	RA-16	–	25.33156° N	76.61814° E	PF, FF1, FF2	PF1 - (0001), FF1 - {11$\bar{2}$2}, FF2 - {11$\bar{2}$1}
Grain-10	RA-16	13A; 13B	25.33156° N	76.61814° E	PF, FF	PF1 - {10$\bar{1}$2}, FF1 - {11$\bar{2}$1}
Grain-11	RA-16	13C	25.33156° N	76.61814° E	PF, FF	PF1 - {10$\bar{1}$0}, FF1 - {10$\bar{1}$1}
Grain-12	RA-16	13D	25.33156° N	76.61814° E	PF, FF	PF1 - {0001}, FF1 - {10$\bar{1}$1}
Grain-13	RA-16	13E	25.33156° N	76.61814° E	PF	PF1 - {10$\bar{1}$2}
Grain-14	RA-16	13F	25.33156° N	76.61814° E	PF, FF	PF1 - {10$\bar{1}$0}, FF1 - {10$\bar{1}$2}
Grain-15	RA-1	–	25.33273° N	76.62492° E	PF	
Grain-16	RA-16	–	25.33156° N	76.61814° E	PDF	PDF1- {10$\bar{1}$4}
Grain-17	RA-16	–	25.33156° N	76.61814° E	PF	PF1 - {10$\bar{1}$0}

Shock Deformation

We found a shock metamorphic overprint in six samples that were all taken within the central depression (Fig. 2A; Table 2). We could not find shock features in the samples from the collar (Lower Bhander Sandstone). We found four grains with PDFs, 13 with PFs, and six with FFs (Table 2). All shock features are decorated with trails of fluid inclusions or micrometer-sized Fe-oxide precipitates. Two of the samples, RA-1 and RA-16, were taken in situ from fractured sandstone outcrops in the central depression. The other samples are float from the crater depression. As this depression is a closed catchment defined by the crest of the collar, the rubble stones could not have been transported over longer distance and definitely originated from the central area of the crater.

Sample RA-1 was taken from the Rewa Sandstone outcrop in the center of the structure (Fig. 2A). The brittle deformation in this sample is intense and partly led to grain crushing. We found only one grain in five thin sections that displays PFs (Table 2). In breccia sample RA-09, a quartz grain with one set of PDF lamellae was found (Fig. 12A). The lamellae are perfectly straight and decorated with fluid inclusions, and have a spacing of 2–3 μm. Breccia sample RA-04 shows PF lamellae at $\{10\bar{1}3\}$ orientation (Fig. 12B). Samples RA-08 and RA-11 are sandstones with a strong brittle deformation overprint, in which PFs along $\{10\bar{1}0\}$ and $\{10\bar{1}1\}$ (Figs. 12C and 12D) and PDFs along $\{10\bar{2}1\}$ were found (Fig. 12E). The latter are very narrow spaced but coated with Fe-oxides. Sample RA-16 is a silicified sandstone that shows a weak shock metamorphic overprint. Shock effects are mainly planar fractures (PFs), from which narrow-spaced lamellae emanate in a comb-like arrangement. These are known as feather features (FFs) and were described in detail in French et al. (2004) and Poelchau and Kenkmann (2011). The formation of FFs is linked to shearing along the associated PFs during shock deformation and subsequent shock release. PFs developed along the (0001) basal plane, $\{10\bar{1}2\}$, $\{10\bar{1}3\}$, and $\{10\bar{1}0\}$, whereas the FFs have $\{10\bar{2}1\}$, $\{11\bar{2}2\}$, $\{10\bar{1}1\}$, and $\{10\bar{1}2\}$ orientations (Figs. 13 and 14; Table 2). The spacing of the PF lamellae ranges from 10 to 50 μm (Fig. 13), whereas FF lamellae spacing is in the order of 5 μm. We found one grain that shows parallel lamellae near a grain boundary with a spacing of 3–4 μm (Fig. 12F). Whether these are PDF lamellae or PFs cannot be ascertained without conducting transmission electron microscopy. Apart from this mild shock metamorphic overprint, the sandstone shows intense grain crushing, intra- and intergranular fracturing, and Boehm lamellae. Stress chains along grain-to-grain point contacts primarily lead to mode I concussion fractures. However, shear fracturing is also abundant.

DISCUSSION

The occurrences of PDFs, PFs, and FFs in quartz grains are generally accepted criteria for the recognition of impact structures (e.g., French 1998; Ferrière et al. 2009; French and Koeberl 2010; Poelchau and Kenkmann 2011). The documentation of distinctive planar features including the measurement of their crystallographic orientations in the quartz lattice unequivocally verifies the hypothesis of Ramgarh being an impact structure, as proposed by Crawford (1972) and later on by many others. The shock metamorphic features were found in situ in outcrops of silicified sandstones as well as in float samples. Only one grain with shock lamellae was found in the Rewa Sandstone outcrop of the center. The predominant finding of PFs with crystallographically controlled FFs suggests strong shearing along PF planes during shock deformation and subsequent unloading of the rocks. The measured orientations (0001), $\{10\bar{2}1\}$, and $\{11\bar{2}2\}$ are typical for PF–FF pairs and indicate a pressure range of $\sim$4–10 GPa (Poelchau and Kenkmann 2011). The scarcity of shock effects in the central uplift of Ramgarh is not unusual when comparing it to similar-sized impact craters. For instance, rocks of the central uplift of the 13.7 km diameter Serra da Cangalha crater, Brazil, also show a minor shock metamorphic overprint (Kenkmann et al. 2011; Vasconcelos et al. 2013). A low shock metamorphic overprint in the center of the structure can be explained by (1) erosion, (2) oblique impact, (3) low cosmic velocity of the impactor, (4) strong shock wave attenuation caused by a porous upper target layer, or a combination of these effects.

Crater Size

Our structural investigations show that Ramgarh is a complex impact structure of approximately 10 km apparent diameter with a central uplift of 3.5–4.0 km diameter (Fig. 15). All previous investigations with the exception of Rakshit (1973) and Dietz and McHone (1974) considered the morphologically elevated collar of Ramgarh the rim of an ancient impact structure. This interpretation is untenable and must be rejected for the following reasons. (1) Craters of 3.5–4 km diameter would not reach 200 m of structural crater rim uplift. For instance, the 3.4 km diameter New Quebec impact structure has a structural rim uplift of roughly 120 m (Grieve 2006), while the 3.8 km diameter Steinheim crater, Germany, and the likewise 3.8 km diameter Flynn Creek crater (USA) have a rim uplift of about

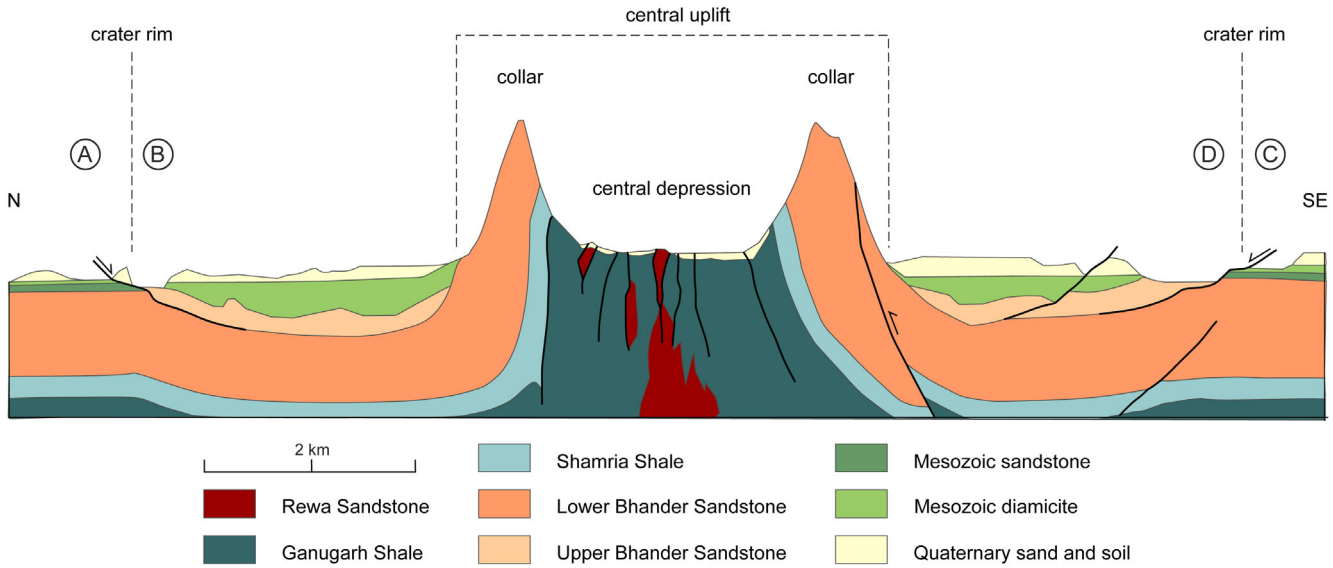

Fig. 15. Schematic cross section through the Ramgarh impact structure. For location of the cross section, see Fig. 1C. Ramgarh is a classical complex crater with a large central uplift that morphologically forms a collar and a central depression. The subdued ring syncline and the eroded crater rim are mostly covered by Quaternary deposits. (Color figure can be viewed at wileyonlinelibrary.com.) (Color figure can be viewed at wileyonlinelibrary.com.)

100 m (Roddy 1977). (2) Most important, the central depression at Ramgarh surrounded by the collar is at a higher elevation than the surrounding plain (Fig. 2). If the collar would represent the crater rim, the crater cavity should be located much deeper than the surrounding plain (Grieve and Pilkington 1996). For instance, at New Quebec, the crater depression is 250 m deeper than the surrounding terrain. At the Steinheim and Flynn Creek craters, the top of the breccia lens in the central depressions is about 150 m and 80 m below the surrounding plain, respectively. (3) The outer slope of the collar of Ramgarh has a slope angle of around 20°-30° (Fig. 2). This is also in contrast to much shallower outer slopes of these aforementioned craters. (4) Strata of the outer collar are dipping too steeply for the periphery of an elevated crater rim (Fig. 5). Crater rims show steeper dips only along the inner slopes of the rim, for example, at Barringer crater, where 20°-56° were determined (Kumar and Kring 2008). (5) There are no signs for a circumferential rim fold along the crest of the collar and no signs for an inverted stratigraphy. (6) None of the structural criteria of impact crater rims, for example, dike injections or thrust wedges (Poelchau et al. 2009; Kenkmann et al. 2014) have been observed along the collar. We conclude that the collar cannot represent the rim of a 3.5–4 km wide impact crater.

In contrast, the collar and the interior depression show the typical structural character of central uplifts (Figs. 10 and 15). Selective erosion of the heavily deformed cores of central uplifts leads to the preferential erosion of the central part, leaving behind an annular collar that corresponds to the outer parts of the central uplift. Examples for this kind of central uplift morphology are the 6 km diameter Jebel Waqf as Suwwan structure, Jordan (Kenkmann et al. 2017), the 13.7 km diameter Serra da Cangalha, structure, Brazil (Kenkmann et al. 2011; Vasconcelos et al. 2013), and the 22 km diameter Gosses Bluff crater, Australia (Milton et al. 1996; Kenkmann et al. 2018). The situation at Ramgarh is very similar. The presence of lithologically incompetent Ganugarh Shales plus increased cataclastic deformation toward the center of the structure allowed for the selective erosion of the central uplift interior causing the relief inversion (Figs. 2 and 15). Using a mean dip of strata in the central uplift of 30°, the stratigraphic uplift is estimated to be approximately 1000 m. This is in good agreement with the empirical relationship of Grieve and Pilkington (1996) between the stratigraphic uplift and crater diameter that suggests 920 m uplift. The apparent size of the crater of approximately 10 km diameter is constrained by the local exposure of large-scale concentric low-angle normal faults defining the apparent rim in the N and SE (Fig. 3E). The hanging wall blocks to these faults are tilted toward the crater interior by some 20°, thus showing synthetic slump rotations (Figs. 5, 6A, 7, and 15). Synthetic tilting is interpreted to have occurred during inward movement and slumping. Down-faulting along the fault during crater modification brought the Upper Bhander sequence at

locations B and D to the altitude of the Lower Bhander Sandstone that forms the footwall of the crater rim fault at locations A and C. The apparent crater rim is further constrained by concentrically trending lineaments that are traceable through the Quaternary cover in the ALOS elevation data (Figs. 4A and 10). The western, northern, and eastern rims are defined well by these lineaments. However, concentric lineaments in the south are rare at a 5 km radius. The crater rim, however, is not defined as a morphologically elevated rim (Fig. 15). This is very similar to the situation at the larger Gosses Bluff impact structure (Milton et al. 1996) that has a pronounced central uplift collar and is devoid of a morphological crater rim.

Nevertheless, the remote sensing results (Fig. 16) show distinctive features in the area of the proposed crater rim that possibly trace the original crater rim. The multispectral data indicate an area of similar multispectral signature appearing as a halo-like feature that surrounds the crater at a distance of approximately 5–7 km (Fig. 16B). The areas beyond this zone can be clearly distinguished, especially in the E and S. The gravity disturbances indicate a weak anomaly within the regional trend that forms a circular feature at a distance of 5–8 km from the center of the structure (Fig. 16C). This feature cannot be explained by topographic effects (Fig. 16A). Due to the low resolution of the gravity data, a clear interpretation is difficult and further geophysical investigations are necessary. In addition, the drainage network shows approximately concentrically oriented drainage divides at a distance of 6–8 km in the S, N, and W (Fig. 16D). Based on landform evolution modeling, Wulf et al. (2019) showed that drainage network and local drainage divides behave very conservatively and are likely to trace original crater structures. Taken separately, the remote sensing results are relatively inconclusive but as a whole, it is evident that there is a significant circular anomaly with a diameter of 10–14 km. Due to the exposure of the crater rim fault in the SE and N sectors at 5 km radius, we use an apparent crater diameter of 10 km for the Ramgarh impact structure.

Oblique Impact

The central uplift of Ramgarh consists of fault-bounded blocks (Fig. 4B). Except for an insignificant E–W trending regional fracture zone that overprints the structure, the fault pattern is consistent with formation of a central uplift in an oblique impact scenario. Systematic deviations from axial symmetry, as indicated for the Ramgarh central uplift, were observed for many eroded central uplifts of terrestrial (Kenkmann et al. 2014, 2017, 2018) as well as Martian impact structures (Wulf et al. 2012). It could be shown that characteristic structural patterns result from oblique impact. The proof of the sensitivity of such structural features with respect to the impact angle and the impact direction was demonstrated by Kenkmann and Poelchau (2009) and Wulf et al. (2012) based on elliptical crater shape and asymmetric ejecta pattern, respectively. At Ramgarh, a bilateral symmetry of the central uplift along the SW–NE direction is a striking first-order structural feature and defines the impact trajectory. This strike-slip fault, denoted as F_t in Fig. 4B, documents that the horizontal component of deformation played an important role during central uplift formation. Faults show a preferred concentric orientation and stacking sequence in the SW sector of the collar, whereas in the NE sector, they exclusively have radial orientations. Using the criteria summarized in Kenkmann et al. (2014), this suggests an oblique impact from the SW toward the NE. The SW sector is the uprange sector, and the NE sector is considered to represent the downrange direction. In the cross range sectors, NW and SE, faults vary between a concentric and a radial trend, and are mostly oblique with respect to the crater center. Strata also show pronounced and regular deviations from concentric strike orientation, in particular in the cross-range sectors. As a consequence of its internal structure, the central uplift has a somewhat rectangular shape, whose SW–NE trending diagonal corresponds to the trajectory and divides the rectangle into bilateral symmetric halves. Like the rectangular central uplift of Serra da Cangalha (Kenkmann et al. 2011), Ramgarh is believed to be formed by a moderately oblique (45°–30°) impact. Craters formed with a strong obliquity (<30°), develop kite-like quadrilateral central uplift shapes by increasing the angle between the downrange sides. When the angle between the downrange sides reaches values of more than 150°, the shape of the central uplift appears triangular. This can be studied, for example, at the Jebel Waqf as Suwwan (Kenkmann et al. 2017), Gosses Bluff (Kenkmann et al. 2018), or Spider crater structures (Kenkmann et al. 2014). At even lower angles of incidence, at very strong obliquity (<15°), when craters obtain elliptical outlines, the central uplift shape becomes a triangle (Kenkmann and Poelchau 2009).

Impact Into Shallow Water?

The lack of a morphologically visible crater rim (Figs. 1B and 15) and the presence of a crater rim fault that is formed as a low-angle normal fault (Figs. 3E and 6) may suggest that the rocks that were building the rim had a low strength and were semi- to

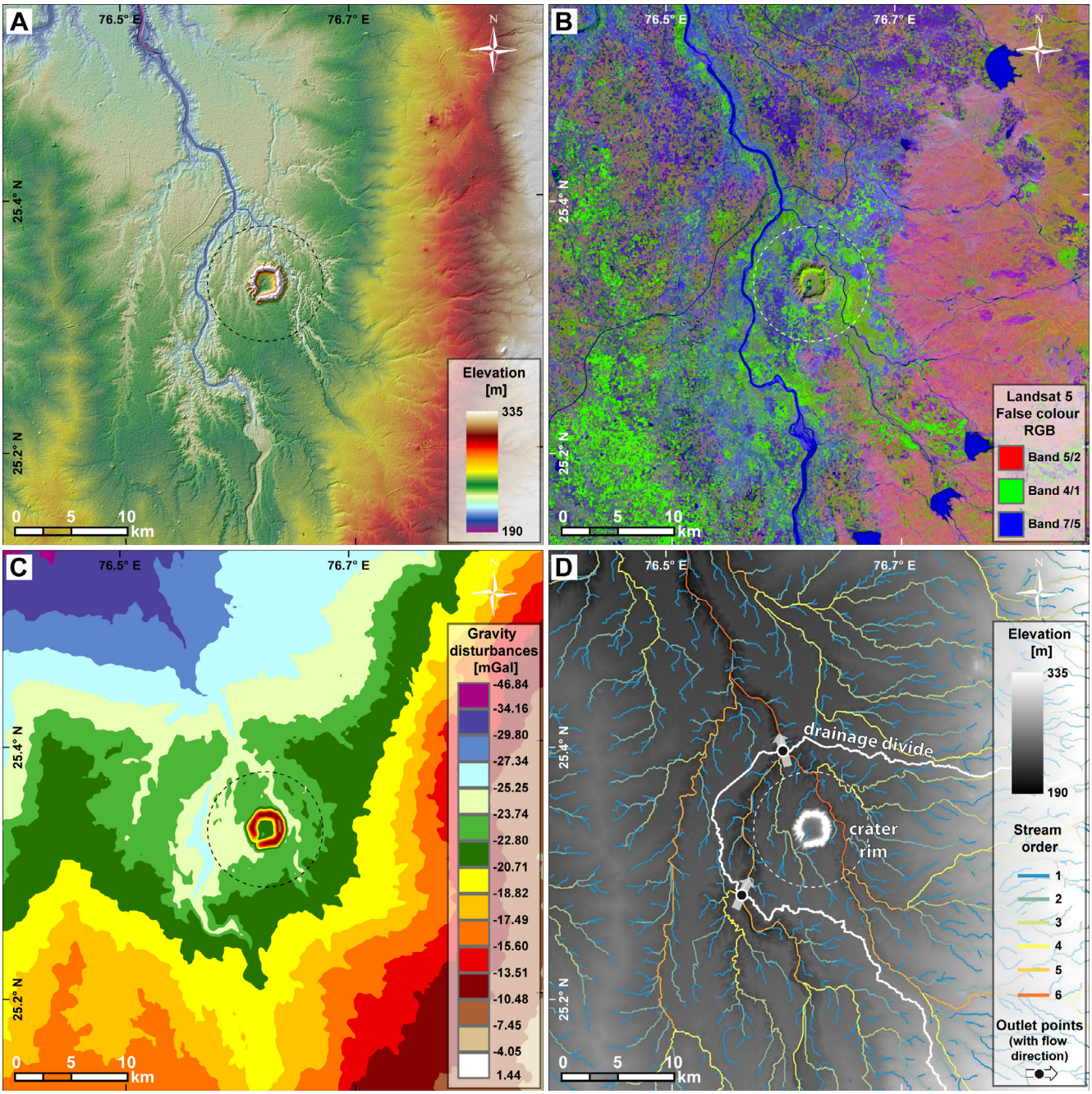

Fig. 16. Maps showing the wider region of the Ramgarh area including A) elevation data (ALOS DEM mosaic superposed on shaded relief), (B) multispectral data (Landsat 5 Thematic Mapper FCC (band combination 5/2, 4/1, 7/5 [scene from 1996]), (C) gravity disturbances (C, GGMplus gravity data; Hirt et al. 2013), and (D) the derived drainage networks and regional drainage divides (superposed on ALOS shaded relief). (Color figure can be viewed at wileyonlinelibrary.com.) (Color figure can be viewed at wileyonlinelibrary.com.)

unconsolidated at the time of the impact. This fits well with the observed soft-sediment deformation near the exposed rim fault at the northern and southern locations along the Kul River. The soft sediment deformation features (Fig. 8) indicate a full water saturation of the sandy substratum and a fluid overpressure when the diamictite and conglomerates were washed over the unconsolidated sand (Fig. 9).

Misra et al. (2019) suggested that the Ramgarh structure is most likely situated on the paleo-channel of the Parvati River, and hence, its formation must have post dated the formation of this river. They suggested

that the impact forced the shift of river courses of the Parvati River and its tributary adjacent to the Ramgarh structure. Indeed, their scenario is compatible with the deposition of conglomerates and diamictites and suggests the involvement of surface water during the evolution of the Ramgarh structure.

However, the preserved gastropod shells (Figs. 9D–F) in well-cemented diamictite beds indicate a Mesozoic age for the deposition of the diamictites and conglomerates, most likely during the Callovian (Upper Middle Jurassic; Table 1). In case the observed diamictite and soft sediment deformation features in the upper part of the sandstone unit are causally connected to the impact event, the soft sediment deformation features would suggest an initial lower energy resurge inflow of water, for example, possibly by an overspill over the crater rim or by the infill with groundwater. The diamictite, in contrast, indicates a high-energy inflow possibly induced by a breach of the crater rim.

Postimpact Sedimentation and Erosion History

Is a Jurassic age for the impact event compatible with its current state of preservation and its morphological appearance? The level of shock metamorphism in the central uplift can be used as a measure for the amount of overburden, and subsequent erosion, which has taken place since the time of impact. The level of shock recorded in the central uplift of the Ramgarh structure is in the order of 7–10 GPa, based on the occurrences of FFs (Poelchau and Kenkmann 2011). Locally, where PDFs are present, the peak shock pressure was probably a few GPa higher. Ferrière et al. (2008) systematically investigated the shock metamorphic overprint of rocks in the central uplift of the similar-sized Bosumtwi impact structure, Ghana (10.5 km crater diameter). The uppermost rocks of the central uplift of this crater structure experienced shock pressures below 30 GPa and the inferred shock attenuation ranged from 5 to 10 GPa at a 200 m core interval. Using this approach, 400–600 m of central uplift material seems to be missing at Ramgarh. A minimum amount of erosion in the center of the dome of 200 m is obvious from the elevation difference between collar and central depression. A strongly oblique impact scenario, in which less energy is transferred to the target (Pierazzo and Melosh 2000), possibly combined with a low cosmic impact velocity would reduce the amount of required erosion. The central uplift structure indicates a moderately oblique impact as detailed above. Likewise, the dominance of FFs as the main shock feature (Figs. 13 and 14) is compatible with such an oblique impact scenario where shear stresses played a dominant role during shock loading and unloading (Stickle and Schultz 2011). Therefore, erosion should have removed at least some 400 m of missing strata and the allochthonous crater fill breccia of the moat.

Is this scenario compatible with the regional geological context and common erosion rates? The presumably most comprehensive compilation of erosion rates (Portenga and Bierman 2011) involving cosmogenic nuclide data from almost 1600 drainage basins suggests 54 $mMyr^{-1}$, in accordance with Hergarten and Kenkmann (2015). Taking into account that the erosion rate is governed by the relief, an erosion rate of 20–30 $mMyr^{-1}$ might be realistic for the flat region near Ramgarh (Hergarten and Kenkmann 2019). If intermittent phases of sedimentation are taken into account, the erosion rate seems to be in rough agreement with an erosion of 400 m since the Jurassic. However, there is little evidence left for a 400 m thick sequence of Mesozoic and Cenozoic sediments that once should have covered Ramgarh. Mesozoic sediments have not yet been reported from elsewhere in the region around Ramgarh. However, in western Rajasthan, depo-centers of Jurassic and Cretaceous sediments are known as the Barmer and Jaisalmer Basin (Ramakrishnan and Vaidyanadhan 2008). Here, the Lathi Formation represents a succession from the Liassic to the Alenium/Bathonian, and the Jaisalmer Formation in both basins was deposited between the Alenium/Bathonium and the Oxfordian/Kimmerigdian. The Lathi Formation comprises ill-sorted sandstones, ferruginous siltstones, purplish white clay and conglomerate, 350 m thick in the basin center, that were deposited in a fluvio-deltaic environment (Ramakrishnan and Vaidyanadhan 2008). These basins are far away from the Ramgarh structure and any lithological correlation is speculative. However, the preserved gastropods embedded in the massive diamictite, and the associated sands with intense soft-sediment deformation may indicate a shallow water fluvio-deltaic environment for the region around Ramgarh at that time. These rocks experienced diagenesis and appear well cemented, and, thus, should have been buried before they became exposed. Cretaceous rocks are known from the Narmada Basin 300 km to the south, the Kutch Shelf 400 km southwest, and the Jaisalmer and Balmer Basins that are situated 500 km west of Ramgarh (Archaryya and Lahiri 1991), but not from the Vindhyan Basin (Bose et al. 2001). The closest distance to the Deccan Trap basalts is some 200 km. Sedimentation in the above-mentioned basins continued during the Paleogene and Neogene. To conclude, the Mesozoic and Cenozoic history of the region is rather obscure but intermittent phases of sedimentation and erosion should have

occurred in the Ramgarh region as well, as indicated by the record of the wider region. Whether the soft sediment structures and preserved diamictites are causally connected to the Ramgarh impact event remains to be proven. If so, it would suggest a deep-reaching layer of unconsolidated sediments. In such a scenario, the crater rim would have been unconsolidated and degraded in the course of the impact event by some sort of resurge in shallow water (Ormö and Lindström 2000).

CONCLUSIONS

The following conclusions can be drawn from our combined analysis of field data, microstructures, and remote sensing data.

1 Ramgarh is an impact structure as confirmed by the discovery of PDFs, PFs, and FFs in quartz grains from sandstones and breccia of the central depression. It is the third impact crater found on the subcontinent of India. Hence, the impact hypothesis proposed by others could be verified.
2 Ramgarh is a complex impact structure of approximately 10 km apparent diameter. The annular topographic high, the landmark of Ramgarh, does not represent the rim of the crater, as was proposed by most previous investigations. This collar is the outer part of a segmented central uplift. The inner part of the central uplift shows relief inversion and forms the central circular depression. The apparent crater rim is exposed at several sites along local river beds as a low-angle normal fault with a ramp-and-flat structure and can be traced as lineaments in remote sensing imagery. Spectral remote sensing data, the local drainage network, and available gravity data of coarse spatial resolution indicate that the crater was originally slightly larger.
3 With the exception of an E–W trending regional fracture zone, the numerous faults of the central uplift are co-genetic with the formation of the central uplift and are indicative for deriving an impact trajectory from SW toward NE. This is indicated by (1) the bilateral symmetry of the central uplift along a SW–NE axis, (2) stacking of reverse faults that preferentially dip SW in the SW uprange sector, (3) the presence of oblique fault-bounded blocks in the cross range sectors, and (4) the narrow-spaced radial arrangement of faults in the downrange sector (NE).
4 Sandstones of the central uplift impregnated by Fe-oxides indicate a hydrothermal mineralization overprint. This was most likely induced by the thermally activated circulation of hydrous brines after the impact.
5 The Ramgarh impact event may have occurred into a shallow water environment as indicated by intense soft-sediment deformation observed at the crater rim and the deposition of diamictite above the rim and within the crater moat. The lack of a morphological crater rim and the presence of low-angle crater rim normal faults support that the uppermost target was unconsolidated at the time of impact. However, further studies are required to prove a causal connection between the soft sediment structures in sandstones and the deposition of the diamictite layer to the impact event.

Acknowledgments—The fieldwork was funded by Innovations fonds-2017 of the University of Freiburg. AA is sponsored through an Alexander von Humboldt Foundation post-doctoral fellowship. Dr. Sanjay Kumar Verma, paleontologist of the Geological Survey of India, is kindly acknowledged for his confirmation of the gastropod identification. We thank Manfred Gottwald for graphically revising the cross section of Fig. 15. Thin sections were prepared by Dagmar Flemming and Herbert Ickler. We are grateful to master students Nabil Sifo and Harith Alkubaisy who drew our attention to the Ramgarh structure in the lecture course "Screening Earth" at the Albert-Ludwigs-University Freiburg. We are very grateful to the reviewers Ludovic Ferrière (Natural History Museum Vienna) and Roger Gibson (Witwatersrand University) for their thorough and extremely detailed reviews that helped to improve the manuscript. We also thank the associate editor Uwe Reimold for manuscript handling and intense copyediting.

Editorial Handling—Dr. Wolf Reimold

REFERENCES

Ahmed N., Bhardwaj B. D., Sajid H. A., and Hasnain I. 1974. Ramgarh meteorite crater. *Current Science* 43:598.

Alberti M., Nützel A., Fürsich F. T., and Pandey D. K. 2013. Oxfordian (Late Jurassic) gastropods from the Kachchh Basin, western India. *Neues Jahrbuch Geologie und Paläontologie Abhandlungen* 270:275–300.

Archaryya S. K. and Lahiri T. C. 1991. Cretaceous palaeogeography of the Indian subcontinent; a review. *Cretaceous Research* 12:3–26.

Balasundaram M. S. and Dube A. 1973. Ramgarh structure, India. *Nature* 242:40.

Bose P. K., Sarkar S., Chakrabarty S., and Banerjee S. 2001. Overview of the Meso- to Neoproterozoic evolution of the Vindhyan basin, central India. *Sedimentary Geology* 41–142:395–419.

Crawford A. R. 1972. Possible impact structure in India. *Nature* 237:96.

Das P. K., Misra S., Basavaiah N., Newsom H., and Dube A. 2009. Rock magnetic evidence of asteroid impact origin of Ramgarh structure. India (abstract #1466). 40th Lunar and Planetary Science Conference. CD-ROM.

Das P. K., Misra S., Newsom H. E., and Sisodia M. S. 2011. Possible planer fractures, coesite, and accretionary lapilli from Ramgarh structure, India: New evidence suggesting an impact origin of the crater (abstract #1294). 42nd Lunar and Planetary Science Conference. CD-ROM.

Dietz R. S. and McHone J. 1974. Impact structures from ERTS imagery. *Meteoritics* 9:329–333.

Dutta A., Raychaudhuri D., and Bhattacharya A. 2018. The Ramgarh structure, Rajasthan, India: a meteorite impact crater? (abstract # 1293). 49th Lunar and Planetary Science Conference. CD-ROM.

Earth Impact Database. 2019. Planetary and Space Science Centre University of New Brunswick Fredericton, New Brunswick, Canada. http://www.passc.net/EarthImpactDatabase/New%20website_05-2018/Index.html. Accessed December 2019.

Ferrière L., Koeberl C., Ivanov B. A., and Reimold W. U. 2008. Shock metamorphism of Bosumtwi impact crater rocks, shock attenuation, and uplift formation. *Science* 322:1678–1681.

Ferrière L., Morrow J. R., Amgaa T., and Koeberl C. 2009. Systematic study of universal-stage measurements of planar deformation features in shocked quartz: Implications for statistical significance and representation of results. *Meteoritics & Planetary Science* 44:925–940.

French B. M. 1998. Traces of catastrophe. A handbook of shock-metamorphic effects in terrestrial meteorite impact structures. LPI contribution 954. Houston, Texas: Lunar and Planetary Institute. 120 p.

French B. M. and Koeberl C. 2010. The convincing identification of terrestrial meteorite impact structures: What works, what doesn't, and why. *Earth-Science Reviews* 98:123–170.

French B. M., Cordua W. S., and Plescia J. B. 2004. The Rock Elm meteorite impact structure, Wisconsin: Geology and shock-metamorphic effects in quartz. *Geological Society of America Bulletin* 116:200–218.

Gottwald M., Kenkmann T., and Reimold W. U. in preparation. Terrestrial impact structures: The TanDEM-X Atlas. Verlag Dr. Friedrich Pfeil.

Grieve R. A. F. 2006. Impact structures in Canada. Geological Association of Canada. *GEOtext* 5:206.

Grieve R. A. F. and Pilkington M. 1996. The signature of terrestrial impacts. *AGSO Journal of Australian Geology and Geophysics* 16:399–420.

Hergarten S. and Kenkmann T. 2015. The number of impact craters on Earth: Any room for further discoveries? *Earth and Planetary Science Letters* 425:187–192.

Hergarten S. and Kenkmann T. 2019. Long-term erosion rates as a function of climate derived from the impact crater inventory. *Earth Surface Dynamics* 7:459–473.

Hirt C., Claessens S. J., Fecher T., Kuhn M., Pail R., and Rexer M. 2013. New ultrahigh-resolution picture of Earth's gravity field. *Geophysical Research Letters* 40:4279–4283.

Kenkmann T. and Poelchau M. H. 2009. Low-angle collision with Earth: The elliptical impact crater Matt Wilson, NT, Australia. *Geology* 37:459–462.

Kenkmann T., Vasconcelos M. A. R., Crósta A. P., and Reimold W. U. 2011. The complex impact structure Serra da Cangalha, Tocantins State, Brazil. *Meteoritics & Planetary Science* 46:875–889.

Kenkmann T., Poelchau M. H., and Wulf G. 2014. Structural geology of impact craters. *Journal of Structural Geology* 62:156–182.

Kenkmann T., Hergarten S., Kuhn T., and Wilk J. 2016. Formation of shatter cones by symmetric fracture bifurcation: Phenomenological modeling and validation. *Meteoritics & Planetary Science* 51:1519–1533.

Kenkmann T., Sturm S., Krüger T., Salameh E., Al-Raggad M., and Konsul K. 2017. The structural inventory of a small complex impact crater: Jebel Waqf as Suwwan. *Jordan Meteoritics and Planetary Science* 52:1351–1370.

Kenkmann T., Rae A. S. P., Cavosie A. J., Cox M. A., Timms N., and Miljkovic K. 2018. The central uplift of Gosses Bluff, Northern Territory, Australia. LPI Contribution 2067. 81st Annual Meeting of the Meteoritical Society. Abstract 6077.

Kenkmann T., Wulf G., and Agarwal A. 2019. India′s third impact crater: Ramgarh, Rajasthan. Large meteorite impacts and planetary evolution VI, Brasília, Brazil: University of Brasília, September 30-October 3, 2019. Abstract 5007.

Khan A. J. 1980. Geology of Ramgarh crater. *Geoviews* 7:173–179.

Kumar P. S. and Kring D. A. 2008. Impact fracturing and structural modification of sedimentary rocks at Meteor Crater, Arizona. *Journal of Geophysical Research* 113: E09009.

Kumar J., Negi M. S., Sharma R., Saha D., Mayor S., and Asthana M. 2011. Ramgarh magnetic anomaly in the Chambal valley sector of Vindhyan basin: A possible meteorite impact structure and its implications in hydrocarbon exploration. *American Association of Petroleum Geologists, Search and Discovery* 80145.

Mallet F. R. 1869. On the Vindhyan series as exhibited in the northwestern and central provinces of India. *Memoir Geological Survey of India* 7:129.

Malone S. J., Meert J. G., Banerjee D. M., Pandit M. K., Tamrat E., Kamenov G. D., Pradhan V. R., and Sohl L. E. 2008. Paleomagnetism and detrital zircon geochronology of the Upper Vindhyan sequence, Son valley and Rajasthan, India: A ca. 1000 Ma closure age for the Purana basins? *Precambrian Research* 164:137–159.

Master S. and Pandit M. K. 1999. New evidence for an impact origin of the Ramgarh structure. *Meteoritics & Planetary Science* 34(Suppl. A):79.

Milton D. J., Glikson A. Y., and Brett R. 1996. Gosses Bluff–A latest Jurassic impact structure, central Australia. Part 1: Geological structure, stratigraphy, and origin. *AGSO Journal of Australian Geology and Geophysics* 16:453–486.

Misra S., Dube A., Srivastava P. K., and Newsom H. E. 2008. Time of formation of Ramgarh crater, India-Constraints from geological structures (abstract #1502). 39th Lunar and Planetary Science Conference. CD-ROM.

Misra S., Panda D., Ray D., Newsom H. E., Dube A., and Sisodia M. S. 2013. Geochemistry of glassy rocks from Ramgarh structure, India (abstract #1020). 44th Lunar and Planetary Science Conference. CD-ROM.

Misra S., Srivastava P. K., and Arif M. 2019. Remote sensing, structural and rock magnetic analyses of the Ramgarh structure of SE Rajasthan, Central India–Further clues to Its impact origin and time of genesis. In *Tectonics and*

structural geology: Indian context, edited by Mukherjee S. New York:Springer Geology. pp. 327–352. https://doi.org/10.1007/978-3-319-99341-6_11.

Murali A. V. and Lulla K. P. 1992. Ramgarh crater, Rajasthan, India: Study of multispectral images obtained by Indian Remote Sensing Satellite (IRS-1A). *Geocarta International* 3:75–79.

Murali A. V. and Williams S. 1990. Ramgarh crater, Rajasthan, India: Study of multispectral data obtained by Indian remote sensing satellite (IRS-1A). *21st Lunar and Planetary Science Conference*. pp. 821–822.

Oldham T. 1856. Remarks on the classification of the rocks of Central India, resulting from the investigations of the Geological Survey. *Journal of the Asiatic Society of Bengal* 25:224–250.

Ormö J. and Lindström M. 2000. When a cosmic impact strikes the sea bed. *Geological Magazine* 137:67–80.

Pareta K. and Pareta U. 2016. Landform classification and geomorphological mapping of Ramgarh Structure, Rajasthan (India) through remote sensing and geographic information system (GIS). *Journal of Hydrology and Environment Research* 4:1–17.

Pierazzo E. and Melosh H. J. 2000. Understanding oblique impacts from experiments, observations, and modeling. *Earth and Planetary Science Letters* 28:141–167.

Poelchau M. H. and Kenkmann T. 2008. Asymmetric signatures in simple craters as an indicator for an oblique impact vector. *Meteoritics & Planetary Science* 43:2059–2072.

Poelchau M. H. and Kenkmann T. 2011. Feather features: A low-shock-pressure indicator in quartz. *Journal of Geophysical Research* 116:B02201.

Poelchau M. H., Kenkmann T., and Kring D. A. 2009. Rim uplift and crater shape in Meteor Crater: The effects of target heterogeneities and trajectory obliquity. *Journal of Geophysical Research* 114. https://doi.org/10.1029/2008JE003235.

Portenga E. W. and Bierman P. R. 2011. Understanding Earth's eroding surface with ^{10}Be. *GSA Today* 21:4–10.

Prasad B. 1984. Geology, sedimentation and palageography of the Vindhyan Supergroup, Southeast Rajasthan. *Geological Survey of India Memoirs* 116:1–107.

Purohit V. and Sisodia M. S. 2013. Universal-stage measurements of planar deformation features in shocked quartz grains recovered from Ramgarh structure (abstract #1151). 44th Lunar and Planetary Science Conference. CD-ROM.

Rakshit A. M. 1973. A short report on the ring structure near Ramgarh, Kota district. Rajasthan. *Geological Survey of India* 15.

Ramakrishnan M. and Vaidyanadhan R. 2008. *Geology of India*. Vol 1 and Vol 2. Bangalore: Geological Society of India.

Ramasamy S. M. 1987. Evolution of Ramgarh dome, Rajasthan: India. *Records of the Geological Survey of India* 113:13–22.

Ramasamy S. M. 1988. The lithostratigraphy and the origin of Ramgarh Dome, Rajasthan, India. *Records of the Geological Survey of India* 114:15–24.

Rana S. and Agarwal V. 2016. Microscopic evidences for the impact origin of Ramgarh structure, Rajasthan, India. *Journal of Indian Geophysical Union* 20:544–550.

Reimold W. U., Trepmann C., and Simonson B. 2006. Comment on "Impact origin of the Ramgarh structure, Rajasthan: Some new evidences by M. S. Sisodia, G. Lashkari, and N. Bhandari. Journal of Geological Society of India, v. 67, pp. 423–431." *Journal of Geological Society of India* 68:561–563.

Roddy D. J. 1977. Tabular comparisons of the Flynn Creek impact crater, United States, Steinheim impact crater, Germany and Snowball explosion crater, Canada. In *Impact and explosion cratering*, edited by Roddy D. J., Pepin R. O., and Merrill R. B. New York: Pergamon Press. pp. 125–162.

Sharma H. S. 1973. Ramgarh structure, India. *Nature* 242:39–40.

Sharma J. K. and Singh S. R. 1970. A note on the geophysical survey in Ramgarh dome. *Geological Survey of India* (unpublished progress report).

Sisodia M. S., Lashkari G., and Bhandari N. 2006. Impact origin of the Ramgarh structure, Rajasthan: Some new evidences. *Journal of Geological Society of India* 67:423–431.

Stickle A. M. and Schultz P. H. 2011. Exploring the role of shear in oblique impacts: A comparison of experimental and numerical results for planar targets. *International Journal of Impact Engineering* 38:527–534.

Stöffler D. and Langenhorst F. 1994. Shock metamorphism of quartz in nature and experiment: I. Basic observation and theory. *Meteoritics* 29:155–181.

Vasconcelos M. A. R., Crósta A. P., Reimold W. U., Góes A. M., and Kenkmann T. 2013. The Serra da Cangalha impact structure, Brazil: Geological, stratigraphic and petrographic aspects of a recently confirmed impact structure. *Journal of South American Earth Sciences* 45:316–330.

Wulf G., Poelchau M. H., and Kenkmann T. 2012. Structural asymmetry in Martian impact craters as an indicator for an impact trajectory. *Icarus* 220:194–204.

Wulf G., Hergarten S., and Kenkmann T. 2019. Combined remote sensing analyses and landform evolution modeling reveal the terrestrial Bosumtwi impact structure as a Mars-like rampart crater. *Earth and Planetary Science Letters* 506:209–220.